**Theses of Doctoral (PhD) Dissertation**

# A Microsurgical Arteriovenous Malformation Model on the Saphenous Vessels in the Rat

**Mohammad Walid Ahmad Al-Smadi, MD, MS**

**Dissertation supervisor: Prof. Norbert Nemeth, MD, PhD, DSc**


**University of Debrecen**

**Doctoral School of Laki Kalman**

**Debrecen, 2024**

# Table of content

**List of Abbreviations**

| | |
|---|---|
| AAV-VEGF: | Anti-Vascular Endothelial Growth Factor |
| Ad-Cre: | Adenovirus-mediated Cre deletion |
| ALK1: | Activin A receptor type II-like 1 |
| ANOVA: | Analysis of variance |
| AO: | Aorta |
| ARdur: | Atrial Reversal peak velocity duration |
| ARUBA: | A Randomized experiment of Unruptured Brain Arteriovenous Malformation |
| AVF: | Arteriovenous Fistula |
| AVM: | Arteriovenous Malformation |
| bAVM: | Brain Arteriovenous Malformation |
| cAVMs: | Cerebral Arteriovenous Malformations |
| CBF: | Cerebral Blood Flow |
| CCA: | Common Carotid Artery |
| CJF: | Carotid Jugular Fistula |
| CO: | Cardiac Output |
| CO2: | Carbon Dioxide |
| CT: | Computed Tomography |
| CVST: | Cerebral Venous Sinus Thrombosis |
| DBP: | Diastolic Blood Pressure |
| DecT: | Deceleration Time |
| ECG: | Electrocardiography |
| EC: | Endothelial Cells |
| EF: | Ejection fraction |
| EI: | Elongation Index |
| $EI_{max}$: | Elongation Index Maximum |
| EJV: | External Jugular Vein |
| ENG: | Endoglin |
| HHT: | Hereditary Hemorrhagic Telangiectasia |
| HHT1: | Hereditary Hemorrhagic Telangiectasia 1 |
| HIF: | Hypoxia-Inducible Factor |
| HIF-1α: | Hypoxia-Inducible Factor 1alpha |
| HR: | Heart Rate |
| HUVEC: | Human Umbilical Vein Endothelial Cells |
| H&E: | Hematoxylin And Eosin. |
| IU: | International Unit |
| IVCT: | Isovolumic Contraction Time |
| IVRT: | Isovolumic Relaxation Time |
| KRAS: | Kirsten Rat Sarcoma Virus |
| LA: | Left Atrium |
| LV: | Left Ventricle |
| LVAWd: | Left Ventricle's Anterior Wall thickness in end-diastole |
| LVAWs: | Left Ventricle's Anterior Wall thickness in end-systole |
| LVEF: | Left Ventricle Ejection Fraction |
| LVET: | Left Ventricle Ejection Time |
| LVIDd: | Left Ventricle’s Internal Diameter in end-diastole |
| LVIDs: | Left Ventricle’s Internal Diameter in end-systole |
| LVPWd: | Left Ventricle's Posterior Wall thickness in end-diastole |
| LVPWs: | Left Ventricle's Posterior Wall thickness in end-systole |

| | |
|---|---|
| LVVOLd: | Left Ventricular Volume in end-diastole |
| LVVOLs: | Left Ventricular Volume in end-systole |
| MCA: | Middle Cerebral Artery |
| MCH: | Mean Corpuscular Hemoglobin |
| MCHC: | Mean Corpuscular Hemoglobin Concentration |
| MCOT: | Mitral Valve Closure To Opening Time |
| MCV: | Mean Corpuscular Volume |
| MEK: | Mitogen-Activated Protein Kinase Kinase Enzyme |
| MMP: | Matrix Metalloproteinases |
| MPI: | Cardiac Performance Index |
| MPV: | Mean Platelet Volume |
| MRI: | Magnetic Resonance Imaging |
| ms: | Milli-Seconds |
| NPPB: | Normal Perfusion Pressure Breakthrough |
| PBS: | Phosphate-Buffered Saline |
| PFG: | Pollock-Flickinger Grading |
| PO: | Post-Operation |
| PO1: | Post-Operation week 1 |
| PO3: | Post-Operation week 3 |
| PO5: | Post-Operation week 5 |
| PO7: | Post-Operation week 7 |
| PO9: | Post-Operation week 9 |
| PO12: | Post-Operation week 12 |
| PV: | Pulmonary Vein |
| PVP: | Polyvinylpyrrolidone |
| PW: | Pulsed-Wave Doppler |
| RBC: | Red Blood Cell |
| RDW-CV: | Red Blood Cell Size Distribution |
| S.D.: | Standard Deviation |
| SBP: | Systolic Blood Pressure |
| SMG: | Spetzler-Martin Grade |
| SRS: | Stereotactic Radiosurgery |
| SS: | Shear Stress |
| SS1/2: | Shear Stress at Half Of The Maximum Elongation Index |
| SV: | Stroke Volume |
| TDI: | Tissue Doppler Imaging |
| TGF- β : | Transforming growth factor-beta |
| VEGF: | Vascular Endothelial Growth Factor |
| VEGF-A: | Vascular Endothelial Growth Factor A |
| VTI: | Velocity Time Integral |
| WBC: | White Blood Cell |

## 1. INTRODUCTION

AVMs are anomalous vascular structures and are made up of a draining vein and a supply artery (1–3). This configuration facilitates a high blood flow rate between the artery and vein with no intermediate capillary bed, creating a complex, entangled structure known as a nidus (4–9). Research suggests AVMs may develop during embryogenesis, specifically in the third week, when the primordial vascular system fails to evolve into a proper capillary network (10–12). Additionally, AVMs can emerge postnatally and exhibit growth following surgical resection or radiotherapy (12,13).

AVMs can manifest various symptoms based on their location. The high arterial pressure flowing through the nidus and draining veins makes these vessels prone to rupture, potentially leading to severe outcomes, including a considerable percentage (38-68%) of new cases exhibiting intracranial hemorrhage, disability, or death (4,13–17). Additionally, AVMs are associated with a range of neurological symptoms, from chronic headaches and migraines to seizures and strokes (18–21). AVMs can also occur outside the brain, affecting the spine, head, neck, limbs, and other organs (22–26).

The study of AVM hemodynamics and rheology is vital, as it is believed that alterations in these areas, especially in venous drainage, may contribute to the formation of AVMs (5,27). Chronic venous hypertension and elevated cerebral venous pressure can result from abnormalities in the cerebrovascular system, such as venous occlusions, narrowing, or absence, which can arise during embryogenesis or after birth. HIF, VEGF, and the angiogenic process can all be triggered by this illness, which can also reduce tissue perfusion (5,27,28). Postnatally, the venous blockage might reactivate dormant arteriovenous connections, potentially leading to AVM formation (27). AVM development appears to persist past the embryonic period, as evidenced by the process of spontaneous growth and regression. Factors such as chronic hypoxia, shear stress, exercise, hormonal changes, and direct trauma can influence AVM morphology, impacting these lesions irrespective of their anatomical position (7,29,30).

Various animal models have been employed to study the hemodynamics of AVMs, each with differing vascular arrangements. These include several anastomosis types between arteries and veins, radiosurgery, gene manipulation, and telangiectasia models. However, these models face challenges, including inaccurate AVM representation and limited data on their role in AVM rupture (31–43). Establishing a model that closely mirrors clinical AVM cases is crucial for better understanding their pathophysiology.

The existence of arteriovenous shunts of various sizes and locations can impact micro-rheological parameters. Past studies have shown a significant increase in red blood cell

aggregation and reduced deformability, changes that continue to evolve in the weeks following the creation of artificial arteriovenous shunts, such as carotid-jugular, femoral, saphenous, and portocaval shunts (44–48). The size, shape, and location of the artificial shunt influence the extent of these changes. In the case of AVMs, which also vary in size, the specific size and vascular structure that led to both hemodynamic and hemorheological disturbances are not yet fully understood.

Diagnosis of cerebral AVMs often occurs incidentally or follows the investigation of acute cerebral hemorrhage, seizures, or chronic headaches (20). These malformations vary in size, location, and vascular structure, necessitating the use of grading scales for classification and management. AVMs are graded according to size, location, and venous drainage using the widely used Spetzler-Martin score system; a higher score denotes a higher risk of microsurgical excision (49). A 10-point scale that took into account variables including age and hemorrhagic appearance was added to the Spetzler-Martin system in 2010 (50–52). Another grading system, the Toronto scale, predicts neurological outcomes post-resection (53).

Treatment approaches for AVMs vary based on their grading and include radiosurgery, microsurgical resection, and endovascular embolization (14,54–56). Surgical removal remains the preferred method for most lesions, though recurrence post-intervention is not uncommon, often due to reperfusion from recanalization or undetected vascular contributions (54,57,58). Despite significant advancements in research and clinical care, the management of AVMs continues to pose challenges, primarily due to the limited understanding of AVM behavior and progression, especially regarding the risk of rupture and aneurysm formation (59–62).

## 2. LITERATURE REVIEW

### 2.1. Arteriovenous malformation - definition

An AVM is a vascular abnormality featured with an atypical entanglement of blood vessels where an artery directly feeds into a nidus, bypassing and avoiding the normal capillary network, and then drains into a vein (Figure 1). Typically, arterial blood flows through a capillary network before entering the venous system (1–3). This disorder can manifest anywhere in the body, but this thesis specifically addresses cAVMs occurring in the brain.

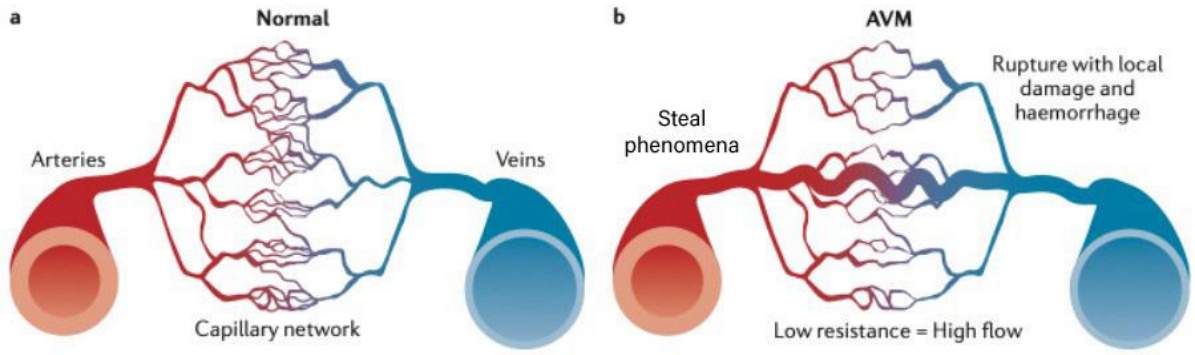


**Figure 1**
Schematic drawing of normal arterio-capillary-venous connection (a) and arteriovenous malformation (b) (63).

AVMs are usually congenital, resulting from vascular development abnormalities during embryonic stages. From an anatomical perspective, a cAVM has a nidus that bypasses capillaries and directs blood flow from arterial feeders into draining veins (64,65). This nidus is a network of interconnected arteries and veins, joined by fistulae that allow blood to rapidly move from the artery to the vein (66). A nidus and early venous drainage are characteristic features of cerebral angiography, the most useful radiological technique for characterizing cAVMs (67). However, neoplastic endothelial cell turnover is absent from vascular tumors or angiomas, which sets them apart from AVMs.

It is crucial to recognize that there are three main kinds of AVMs in the brain: pial AVMs are found in the cortical area, cerebral AVMs are found in the supratentorial region, and general brain AVMs can occur anywhere in the brain. These categories are essential to the management of AVMs since the location of the lesion greatly affects the available treatments. For instance, pial AVMs are generally more accessible for surgical intervention.

## 2.2. Prevalence

The actual prevalence of cAVMs in the general population remains unknown, despite parallels in their development across males and females (68,69). The estimation of AVM prevalence in populations through prior attempts has been hindered by biased reporting methods or small sample numbers (68,70). It is estimated that the prevalence of AVM is probably less than 10.3 per 100,000 people based on incidence data from the New York Island AVM Study (68). However, it is likely that different global populations have variable incidence and prevalence rates of AVMs (71–73). Furthermore, it is difficult to ascertain the actual prevalence of asymptomatic AVMs due to the unintentional identification of these lesions brought about by the availability of brain imaging for unrelated conditions (74,75).

As a result, researchers believe that there is a far greater true frequency of AVMs in the general population. Only 12% of AVMs are thought to develop symptoms, according to a historical autopsy study from 1978. However, more recent research has not supported this number (76).

## 2.3. Diagnosis and presentation

Depending on their location and size, cAVMs might provide a significant risk for rupture. In addition to the associated symptoms of headaches, muscle weakness, and seizures, this may cause an intraventricular or intracerebral hemorrhage (77). In children and young adults, the most common cause of hemorrhagic stroke is AVM rupture (78,79). An annual hemorrhage rate ranging from 2% to 4% and an approximate 1% death rate across AVMs of all diameters have been documented by meta-analyses and studies looking at the natural development of AVMs (80–82).

Furthermore, an intact AVM may produce symptoms as a result of its mass effect or by inducing cerebral ischemia in the tissues around it (83). All age groups are susceptible to AVMs. Still, the majority of symptoms are typically seen in young adults in their third or fourth decade of life (84). Apart from strokes, localized neurological impairments, headaches, seizures, and spontaneous intracerebral or subarachnoid hemorrhages are other symptoms that can be associated with AVMs.(85) However, roughly 88% of AVM patients do not exhibit any symptoms, making the detection of AVMs a difficult task (86).

This is despite the vast range of possible symptoms. AVM diagnosis was formerly thought to be best achieved using angiography (87). MRI and CT, in particular, have become the preferred techniques for locating, displaying, and diagnosing AVMs in patients, nevertheless, as a result of technical developments in radiology (88,89).

## 2.4. Etiology

It is still unclear whether fundamental factors lead to the creation and rupture of cAVMs. Congenital anomalies were once thought to be the exclusive cause of AVM formation (90). However, recent studies have shown that AVM growth and rupture are dynamic, intricate processes in which hereditary factors may play a minimal impact (91). HHT and capillary malformation–arteriovenous malformation syndrome are two examples of AVM cases with a genetic component, accounting for around 5% of all AVM cases. Both conditions have autosomal dominant inheritance patterns (92,93).

Identifying the precise genes linked to the formation of cerebral AVM in these situations has been the focus of preclinical research efforts. The likelihood of cerebral AVM formation is known to be elevated by congenital alterations in the RAS and TGF-β vascular signaling pathways (94,95). This work has primarily focused on genes that encode proteins, such as ENG and ALK1 (92,93,96).

There are no family links in about 95% of AVM cases (97). The causes that led to the formation of these sporadic AVMs are mainly unknown. Somatic mutations in the RAS-MAPK pathway have been linked in recent studies to the emergence of sporadic AVMs (98,99). The ruptured AVM vasculature has also been found to have abnormal endothelial and mural cells (100,101).

As will be further explained in this context, scientists are examining a number of vascular observations, such as endothelial hyperplasia, the potential for cells to breach the blood-brain barrier, and a decline in the populations of smooth muscle and pericytes. These investigations seek to develop prophylactic treatments against AVM rupture as well as potentially identify the mechanisms behind the creation of AVMs (102–105).

## 2.5. Pathogenesis

The exact formation mechanism of cAVMs is not definitively understood. Some cAVMs are observed at the boundaries of arterial territories, leading to the hypothesis that they may originate during fetal development due to the persistence of arterial connections, bypassing the usual remodeling process.

### *2.5.1. Cerebral blood vessel formation*

Vasculogenesis and angiogenesis are the two phases that make up the formation of cerebral vascular structures. A primary vascular plexus is formed in the initial stage by the

formation of primordial endothelial cells (67,106). The second step involves remodeling this plexus, including forming new branches, branch shortening, and supporting newly developed vessels (107). This process leads to the coordinated development of veins and arteries and ongoing adjustments to vessel branching. Cerebral cortical vascular development includes two aspects: ventriculomegaly and ventriculomegaly branches (107,108). Whereas ventriculomegaly branches move in the other direction, ventriculomegaly branches radiate outward from the ventricle to the pial surface. Radial neurogenesis and, thus, vascular development take place together.

The molecular environment plays a crucial role in vascular development. During the early stages of corticogenesis, high levels of VEGF family molecules are present in the ventricular zone, which is essential for the migration of centripetally directed vessels (106). Angiogenesis is induced by growth factors such as VEGF and signaling molecules like MMP, as will be further discussed in the section on genetic involvement (106).

Prior to recently, cAVMs were thought to be congenital lesions brought on by aberrant vascular development. This opinion is reinforced by the correlation between cAVMs and well-known genetic diseases such as ataxia telangiectasia, Osler-Weber-Rendu syndrome, Sturge-Weber syndrome, and HHT (106). However, only 5% of cAVMs have a genetic mutation found in them, meaning that most of them are sporadic in nature. Recent evidence suggests that cAVMs are dynamic lesions that can change in size, spontaneously regress, and even reappear after treatment and apparent obliteration. An analysis of the literature turned up 12 cases of recurring cAVMs, nine of which were patients under the age of 20. This implies that cAVMs may be prone to recurrence instead of being entirely congenital, potentially including a "primed" or immature neurovasculature (106,109).

### *2.5.2. Hypoxia, venous occlusion, and angiogenesis*

Angiogenesis is known to be induced by hypoxia through upregulation of VEGF. When tissue becomes oxygen-deprived or anoxic, it leads to an increase in VEGF-A expression. Cells deprived of oxygen release HIF-1α, a transcription factor that plays a crucial role in regulating the expression of various angiogenic genes, including the stimulation of VEGF-A production. It is interesting to note that de novo cAVMs have been seen to develop later in life, frequently while cerebral ischemia or infarction is present. Iatrogenic insults or ischemic stroke can cause these conditions.

CVST is a condition that can lead to venous occlusion and subsequent cerebral ischemia, and angiogenesis is induced as a response to the resulting hypoxia. Although CVST

is rare in childhood, it is conceivable that such an event during childhood could induce angiogenesis, potentially leading to the formation of cAVMs. However, there have been no investigations to determine how frequently children with CVST go on to develop cAVMs.

Fever, infection, head or brain trauma, and dehydration are a few risk factors for pediatric CVST. Risk factors for neonatal CVST are similar and include infection, severe dehydration, and hypoxia in the early life. These risk factors hypothetically could trigger CVST, creating a hypoxic environment in the brain that subsequently initiates angiogenesis and the development of cAVMs. Moreover, features indicating venous occlusion on angiograms might be associated with a higher likelihood of angiogenesis.

### 2.6. Treatment and management

Currently, various therapeutic options are accessible for addressing AVMs, including neurosurgery, embolization, and SRS. Despite the availability of these diverse treatment modalities, certain studies have suggested that a conservative medical management approach may yield superior outcomes for patients compared to interventions performed prior to AVM ruptures (86,110). Conservative treatment has been supported by numerous references to the ARUBA (A Randomized experiment of Unruptured Brain Arteriovenous Malformation) experiment. In contrast to patients who received prophylactic interventional therapy for unruptured AVMs, both short-term (111) and long-term (110) data from this trial have indicated a significant reduction in the risk of mortality and stroke in patients treated with medical management alone in contrast to those who were on prophylactic interventional therapies for unruptured AVMs.

A follow-up research carried out in 2022, however, refuted these conclusions and hypothesized that the ARUBA trial's conservative AVM treatment approaches may have contributed to a rise in the frequency of AVM ruptures and the death that goes along with them. The AVM rupture and fatality rates among patients were found to have increased thrice in this study when comparing the rates before and after the ARUBA experiment (112). Innovative AVM treatments are desperately needed, even if conservative treatment is the best option for patients. This is because current therapeutic techniques frequently result in less than ideal outcomes.

For instance, endovascular embolization has been associated with a heightened risk of surgical complications compared to its curative objectives (113). Stereotactic radiosurgery, while effective, may require up to two years post-surgery to achieve complete AVM obliteration (114). Moreover, patients frequently develop post-treatment seizures, the underlying causes of

which remain incompletely understood (115). Further complicating AVM treatment is the need for established treatment guidelines (116). Consequently, there is an urgent demand not only for novel AVM treatment strategies but also for establishing universally accepted treatment protocols.

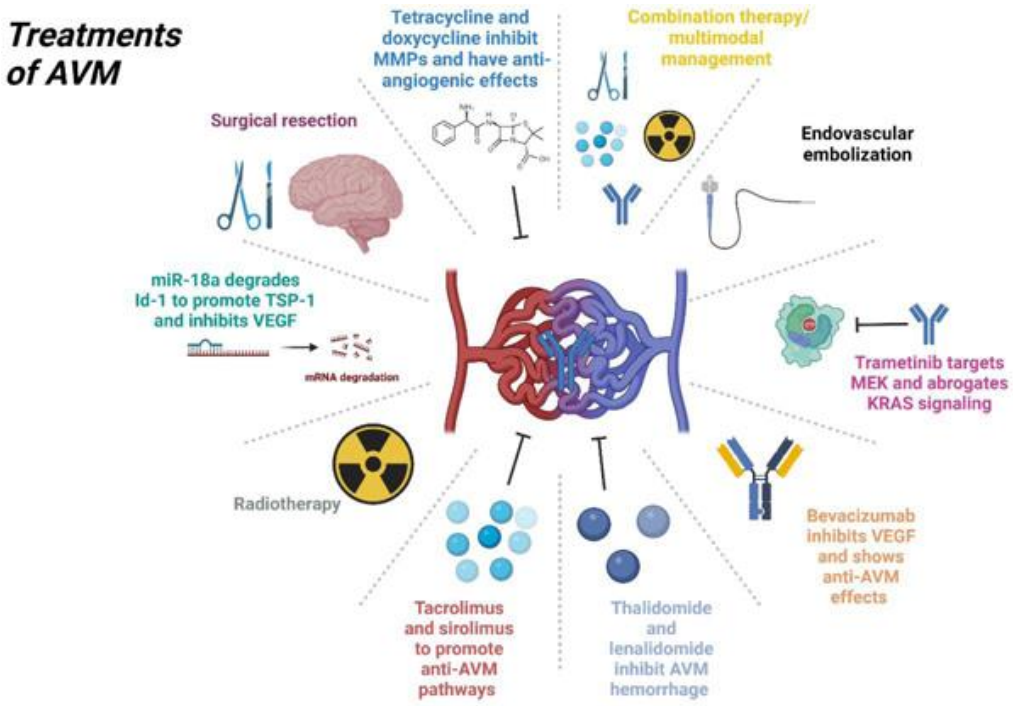


**Figure 2**
Schematic drawings of the main treatment methods of AVM (117)

### 2.7. Preclinical, experimental models of AVMs

Over the past five decades, bAVMs models have been significantly refined in response to scientific and clinical imperatives, aiming to replicate human bAVMs faithfully and consistently. Initially, these models relied on surgical techniques to create arteriovenous fistulas and shunts, enabling the study of hemodynamic alterations in various animal models (5). Extracranial anastomosis of carotid-jugular vessels was frequently used in the creation of arteriovenous fistulas and shunts. This technique was originally described in 1948 with the purpose of examining hemodynamic patterns linked to seizure disorders and cognitive impairment (118). Subsequently, this technique was adapted to investigate bAVM hemodynamics.

### *2.7.1. In vivo models*

*2.7.1.1. Surgical models*

An arteriovenous fistula was used in one of the first in vivo models to mimic the pathophysiology of bAVM in rhesus monkeys to examine hemodynamic alterations. Blood was diverted from the circle of Willis to the internal jugular vein (Figure 3) (119,120). To simulate the physiology of bAVM and evaluate the safety and effectiveness of treatments such as radiosurgery and endovascular embolotherapy, this method was expanded to include mice, cats, and larger animals like sheep (120–123).

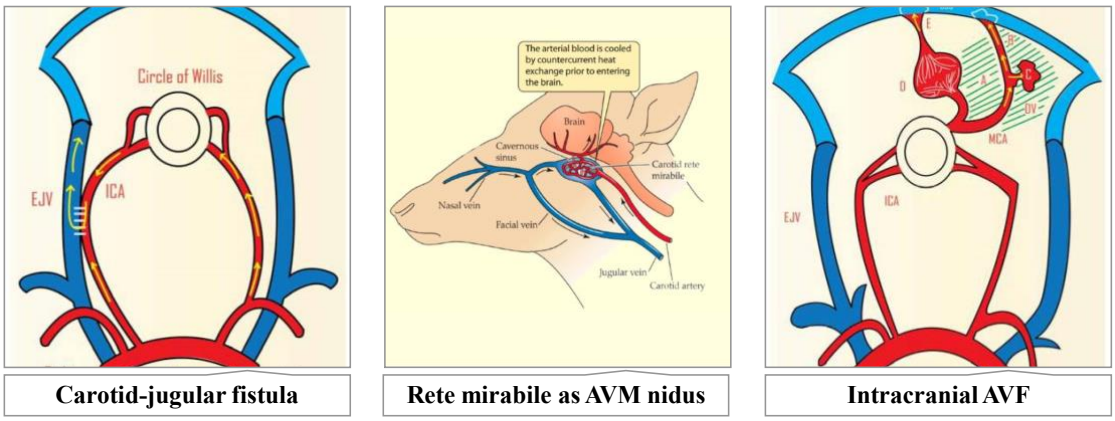


**Figure 3**

Schematic drawings of main experimental surgical approaches to form an AVM model (40,122,124).

A carotid-jugular anastomosis rat model of bAVM was created by Morgan et al. in 1989, and the results of the model's hemodynamics were quite similar to reports from human clinical trials (121). However, it is imperative to acknowledge that each model system possesses intrinsic constraints. Although the placement of a fistula or shunt surgically can mimic some features of blood vessel maneuverability hemodynamics, it might not be able to answer basic concerns about the underlying biology of bAVM development.

A pivotal development in the history of modeling bAVMs involved the identification of a distinctive anatomical feature in swine, known as a rete mirabile. This structure comprises a complex network of interconnected micro arteries and bears angiographic resemblances to certain aspects of human bAVMs (125–127). Nevertheless, this structure lacks arteriovenous connection in the biological context of bAVM. In order to mimic this vital characteristic, the rete mirabile must be surgically punctured in order to redirect blood flow to the cavernous sinus. (126). Notably, the rete mirabile is located extracranially.

While the swine-based model does exhibit essential human bAVM characteristics, such as comparable hemodynamics, it also presents several limitations. The model relies on surgical alteration of the rete mirabile, which is not intricately involved in cerebral microcirculation (125,127). In swine models, surgical puncture of the rete mirabile resulted in specific ocular problems, such as proptosis, chemosis, and sub-conjunctival hemorrhage in the same eye, along with shunt blockage within 5-7 days (125,127). This model is most appropriate for short-term studies on the biology of bAVMs because of the comparatively short time interval before artery closure.

To address the requirement for long-term models, scientists have created a method that uses the rete mirabile to investigate the principles behind vascular remodeling and evaluate the effectiveness of liquid embolization. A chronic bAVM model was established by delaying the time to vessel occlusion and making a fistula big enough to allow for vascular remodeling within the rete mirabile while maintaining patency. Using this chronic technique on swine-based models has proven very helpful in assessing the safety and effectiveness of liquid embolization agents, including n-butyl cyanoacrylate, copolymer ethylene vinyl alcohol, and other new chemicals. The outcomes show that surgically produced bAVMs can be effectively embolized within the rete mirabile with favorable biocompatibility (126,128–130).

As previously mentioned, various animal models, including swine, feline, murine, and larger animals like sheep, have employed extracranial shunts and fistulas to investigate the biology of bAVMs and assess therapeutic interventions. However, these models must directly address the intricacies of intracranial bAVMs or their interactions with cerebral microvasculature.

Pietila et al. (2000) broke new ground in creating a canine model for bAVMs by identifying this vacuum in the scientific literature. This novel model aimed to accurately mimic the angiographic and histopathologic features of real intracerebral bAVMs (124). The development of this canine model was reliant on a number of critical conditions that were necessary to replicate the biology of human bAVM biology. These requirements included the existence of medium-sized to large-sized cerebral arteries, cerebral hemodynamics, and angioarchitecture similar to those found in humans, and the development of angiogenesis to demonstrate aberrant wall formations surrounding the bAVM (124).

*2.7.1.2. Genetic Models*

Genetically engineered mouse models play a crucial role in basic and translational research, offering valuable insights into the molecular and genetic basis of bAVMs, particularly concerning HHT (40,131). To investigate the etiology of HHT1, a mouse model with a

heterozygous knockout of endoglin (Eng+/−) was developed, enabling the study of changes in cerebral vasculature.(40) This model revealed that heterozygous mice exhibited vascular anomalies, including bAVMs, although only 30% showed these anomalies, suggesting a partial role of endoglin in bAVM development (40). In contrast, homozygous wild-genotype mice displayed no vascular anomalies. This indicates that additional factors might be necessary for the full development of bAVMs, as evidenced by the low incidence in heterozygotes (40).

Another approach involved a transgenic Cre-recombinase inducible endoglin knockout model (132). In this model, endoglin was knocked out in vascular smooth muscle cells by tamoxifen injection, and 90% of postnatal animals had a bAVM phenotype (132). Further studies incorporated VEGF, demonstrating that its administration to heterozygous mice led to the development of abnormal cerebral vasculature, including bAVMs, in 8 out of 9 mice, whereas homozygous controls did not develop such vasculature (133). This result points to a synergistic effect between endoglin knockout status and VEGF, necessitating more research to understand the molecular interactions driving these vascular changes (133).

Another gene implicated in HHT is Alk1 (134,135). Three phenotypic groups were obtained from a model in which Alk1 was conditionally knocked out using Cre-recombinase: one group had no lesions, another had arteriovenous fistulae and a third had AVMs (135). The inconsistent illness manifestation among mice with the genetic mutation, despite the fact that a subset of animals with this conditional knockout developed AVMs, is a noteworthy drawback of GEMMs (Figure 4).

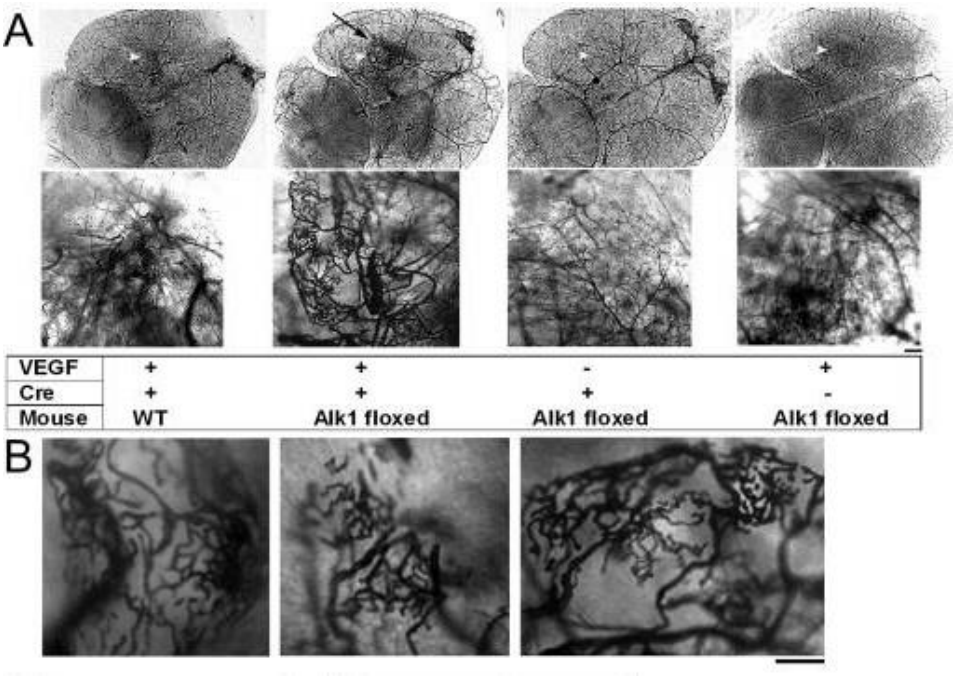

**Figure 4**

Vessel imaging demonstrates distinct cerebrovascular anomalies in the Alk1-depleted area following VEGF stimulation. (A) At the Ad-Cre and AAV-VEGF injection site in Alk1-floxed mouse brains, the formation of large, entangled vessels, similar to a bAVM, was observed (indicated by a black arrow). The absence of VEGF alongside Alk1 deletion (only Ad-Cre injection) did not alter the cerebrovascular structure. The lower images are magnified views of the angiogenic areas shown in the upper images. The scale is set at 100 μm, and injection locations are marked by white arrowheads (B) Atypical vascular formations from three different Alk1-floxed mice injected with Ad-Cre and AAV-VEGF are shown. Each image is scaled at 100 μm. Additional research has employed the conditional knockout model to investigate hemorrhagic stroke and bleeding associated with AVMs (136).

Further studies have used the conditional knockout model to study bleeding and hemorrhagic stroke related to AVMs. The AVM phenotype that is seen when Alk1 loses function is successfully replicated in these investigations (136,137).

TGF-β has been identified as a critical factor in neurovascular development (138). An inducible Cre-recombinase conditional knockout model targeting itgb8 and smad4 was used to assess the role of integrin-8-mediated TGF-β activation in cerebral neoangiogenesis. This study revealed that disruption of TGF-β signaling in the context of VEGF-induced angiogenesis led to vascular morphological changes akin to capillary dysplasia and bAVM. This evidence suggests that integrin 8 plays a significant role in regulating TGF-β activation during cerebral angiogenesis and its disruption could result in AVM-like phenotypes (139). Additionally, studies on genetic mutations in KRAS (G12D or G12V) in vivo in mice and zebrafish revealed that activating these mutations using a tamoxifen-inducible Cre-recombinase system led to the induction of bAVMs (140).

Gain-of-function mutations in KRAS (G12D or G12V) in adult and postnatal mice as well as zebrafish have been the subject of several genetic studies (98,140,141). In these investigations, activating mutations in KRAS alone produced bAVMs in both mice and zebrafish using a tamoxifen-inducible Cre-recombinase transgenic system (140). Constitutively active Notch4 (int3) mutations have also been associated with developing an AVM-like phenotype in mice (142). Mutants exhibiting vascular anomalies and arteriovenous shunting in animals with tetracycline-induced Notch4 expression demonstrated a striking resemblance to the primary abnormality found in human bAVMs (142).

Conditional Rbpj deletion in cerebral endothelium related to Notch1 signalling produced arteriovenous shunting, increased vessel density, and abnormal vascular shape, which

are features of AVM in early postnatal animals (143) These findings highlight the significance of Rbpj as a mediator in Notch1 signaling and its role in the development of AVMs.

### *2.8.2. In vitro models*

Many in vitro models have also been created, even though in vivo models offer a wealth of information regarding the pathophysiology of bAVM. These models are intended to assess various elements of the disease, imaging, therapy materials, and therapeutic efficacy (144–146).

To address some limitations of in vitro models, particularly in replicating anatomical features of bAVMs, Kaneko et al. (2020) created a three-dimensional (3D) printed model of bAVM using patient angiography (147). With hollow nidus channels included into the internal structure, this novel model accurately mirrored the vascular shape of real patient data when used to simulate endovascular methods for treating bAVMs (147). This development represents the first of its kind to integrate such detailed nidus architecture into a model.

Human ECs with KRAS mutations were used to create an AVM-on-a-chip model replicating important AVMs field features (148). This model made use of immortalized HUVEC that were cultivated with fibroblasts in fibrin hydrogels on a microfluidic device. The cell lines expressed either wild-type or doxycycline-inducible mutant KRAS. According to AVM biology, the mutant ECs showed substantial vessel expansion, increased branching at junctions, and higher permeability. The injection of a MEK inhibitor resulted in the correction of barrier integrity defects in mutant ECs by impeding signaling through mutant KRAS (148).

## 2.9. Grading and Classification of AVMs

cAVMs are categorized or graded using a variety of techniques. They can be separated into grades to determine the chances of therapeutic success and dangers and into anatomical grades that provide information on topology and morphology.

### *2.9.1. Spetzler-Martin Grade*

The SMG.25 is the most often used cAVM classification scheme (Table 1). Its development made making management choices based on morbidity and mortality concerns easier. To decide whether to operate, the immediate risks of surgery are weighed against the long-term consequences of not treating the condition (49). A flawless grading system would indicate the level of difficulty associated with a single cAVM's safe surgical excision. Even

though it would be easy enough to use everywhere, it would give a reasonable estimate of mortality and morbidity. There was no such grading scheme in place before the SMG.25 (49).

**Table 1.:** Spetzler-Martin Grade (49)

| Size of AVM | Score |
|---|---|
| Small | 1 |
| Medium | 2 |
| Large | 3 |
| **Eloquence of adjacent brain *** | |
| Non-eloquent | 0 |
| Eloquent | 1 |
| **Pattern of venous drainage #** | |
| Superficial | 0 |
| Deep | 1 |
| **Grade = Total score** | |

*Eloquent = sensorimotor, language and visual cortex; hypothalamus and thalamus; internal capsule; brainstem; cerebellar peduncles; deep cerebellar nuclei. # Superficial = cortical venous system & cerebellar hemispheric veins (which drain directly into the straight or transverse sinuses), the rest is deep.

Spetzler and Martin's extensive encounters in managing cAVMs served as the basis for identifying the components of the SMG.25. As numerous factors were interconnected, the primary factors influencing the assessment of resection complexity, including the count of feeding arteries, blood flow volume within the cAVM, degree of arterial diversion, dimensions, positioning, functional significance of adjacent brain tissue, venous drainage pattern, and surgical accessibility, were condensed and rationalized into venous drainage pattern, size, and eloquence (49).

To assess the predictive accuracy of the SMG, a retrospective evaluation was conducted on 100 consecutives completely removed cAVMs. The grading of these cAVMs was determined based on their imaging characteristics and surgical complications, which were further categorized into minor and major deficits and mortality cases. Neurological deficits that lasted less than three days were excluded from the analysis. Notably, there was a strong correlation between the occurrence of neurological complications and the grade of cAVMs. For instance, when Grade I lesions were surgically removed, minimal neurological deficits were observed. To assess the consistency and dependability of the grading system, one of the study's

authors and two neurosurgeons independently assessed 25 cAVM angiograms. The agreement among all observers was found to be excellent (49).

The SMG score is determined based on several factors, including the eloquence of the neighboring brain tissue (considered eloquent if located in critical areas such as the hypothalamus, brainstem, thalamus, cerebellum, language, visual, sensory, or motor cortex), the type of venous drainage (whether it's deep or superficial), and the size of the nidus (classified as <3 cm, 3-6 cm, or >6 cm) (64). These factors help assess the potential surgical risks and outcomes for cAVMs. The grading system is specifically designed for cAVMs and aids in making treatment decisions by estimating the risk of surgical complications and mortality.

The supplemental SMG was developed to enhance the accuracy of predicting post-operative neurological outcomes (51). This supplementary grading system complements the original SMG by incorporating additional factors, including the extent of nidus diffuseness, the presentation with hemorrhage, and the patient's age. By considering these additional variables, the supplemental SMG provides a more comprehensive assessment of surgical risk, resulting in a more even distribution of risk categories (51). It also greatly improves the accuracy of preoperative risk prediction and aids in refining patient selection for surgical interventions.

### *2.9.2. Pollock-Flickinger Grade*

The PFG system was developed to assist in choosing between radiosurgery and surgery, as well as to predict the likely outcomes following radiosurgery (149). This grading system is based on a formula that takes into account the location of the cAVM, the age of the patient, and the volume of the cAVM (Table 2.). When it comes to predicting the outcomes of radiosurgery, the SMG is not a dependable tool because it does not factor in elements such as radiation dose and specific location, which are critical in this context.

**Table 2.:** Calculating the Pollock-Flickinger grade (149).

| Characteristic | Coefficient |
|---|---|
| AVM volume (cm3) | 0.10 |
| Patient age (years) | 0.02 |
| AVM location #<br>Frontal or temporal = 0<br>Parietal, occipital, intraventricular, corpus callosum, | 0.30 |

| | |
|---|---|
| or cerebellar = 1<br>Basal ganglia, thalamic, or brainstem = 2 | |

AVM score = (0.1) (AVM volume) + (0.02) (patient age) + (0.3) (AVM location),

# When an AVM involves multiple sites, fractional values are used according to the number of sites (0.5 for two sites, 0.33 for three sites)

A multivariate analysis was conducted to establish this grading system, utilizing data from 220 patients who were treated between 1987 and 1991 (149). The primary outcome measure was excellent patient outcomes, defined as complete cAVM obliteration following treatment with no new neurological deficits. Another group of 136 cAVM patients, treated between 1990 and 1996 at a different medical facility, was used to validate the PFG. This validation demonstrated that the PFG could effectively predict patient outcomes following radiosurgery ($p<0.001$) (149). Patients with a PFG score of $\leq 1$ consistently achieved excellent outcomes, whereas this outcome was observed in only 39% of those with a score >2. The PFG system showed a strong correlation with patient outcomes after a single-session radiosurgery. In contrast, the SMG ($p=0.13$) did not exhibit a significant correlation with excellent patient outcomes. Some limitations of the PFG include its development in centers using the gamma knife (so its applicability to radiosurgery delivered by a linear accelerator is unclear), its prediction of outcomes after a single radiosurgery session (rather than for an entire course of treatment), and its retrospective development and application.

### *2.9.3. Embolisation Prognostic Risk Score*

The Embolisation Prognostic Risk Score was introduced to evaluate neurological deficits' severity, predictors, and incidence following adjuvant embolization (150). To establish this scoring system, a multivariate analysis was conducted on data from 202 patients who underwent 377 embolization procedures. Several risk factors for immediate post-embolization neurological deficits were identified, including eloquent location, small and large size of the AVM, complex vascular anatomy requiring multiple embolization procedures, and deep venous drainage. Notably, a significant portion of patients who experience deficits after treatment recover over time. Therefore, the applicability of this score is limited to a specific subset of patients.

## 3. OBJECTIVES

1. Our main goal was to establish an arteriovenous malformation (AVM) model in rats that doesn't cause prompt significant hemodynamic and cardiac alterations but is feasible for follow-up of the AVM's progression.
2. In a 12-week follow-up period to study hemodynamic parameters, echocardiography variables.
3. To analyze micro-rheological and hematological alterations in the presence of the artificial AVM during the follow-up period.
4. At the end of the 3-month follow-up period we conducted a detailed morphological and histomorphological analysis of the AVM with a focus on vascular regeneration/remodeling processes.

## 4. Materials and Methods

### 4.1. Experimental Animals

In compliance with national (Act XXVIII of 1998 on the protection and sparing of animals) and EU (Directive 2010/63/EU) regulations, the experiment was registered and approved by the University of Debrecen Committee of Animal Welfare and by the National Food Chain Safety Office (registration Nr. 25/2016/UDCAW, 25/2022/UDCAW).

In this investigation, sixteen female Sprague Dawley rats (10–12 weeks old, body weights: 293.21±10.33) were used. A group with arteriovenous malformation (AVM, n = 8) and a sham-operated control group (Sham, n = 8) were randomly assigned to them. The rodents were housed in typical cages with free access to commercial rat chow and water, and they have exposed today and night light cycles every twelve hours.

### 4.2. Operative techniques

We ensured a sterile surgical environment for each rat by setting up sterilized instruments and keeping the operating space clean. A combination of 0.05 mg/kg atropine, 10 mg/kg xylazine, and 100 mg/kg of ketamine was administered intraperitoneally to anesthetize the rats. The rats also had an intravenous infusion of heparin at the recommended 80 IU/kg dosage to avoid thrombotic events. The lateral vein of the tail was fitted with a safe, 26-gauge cannula in the event that perioperative medication requirements existed.

The lower abdomen, inner thighs, and upper legs were shaved and treated with betadine for infection after anesthesia. Betadine and sterile gauze were used to prepare the surgery site carefully. A 3-centimeter incision was made obliquely over the right knee. The right saphenous veins and arteries in the AVM group were the targets of the intervention (Figure 5).

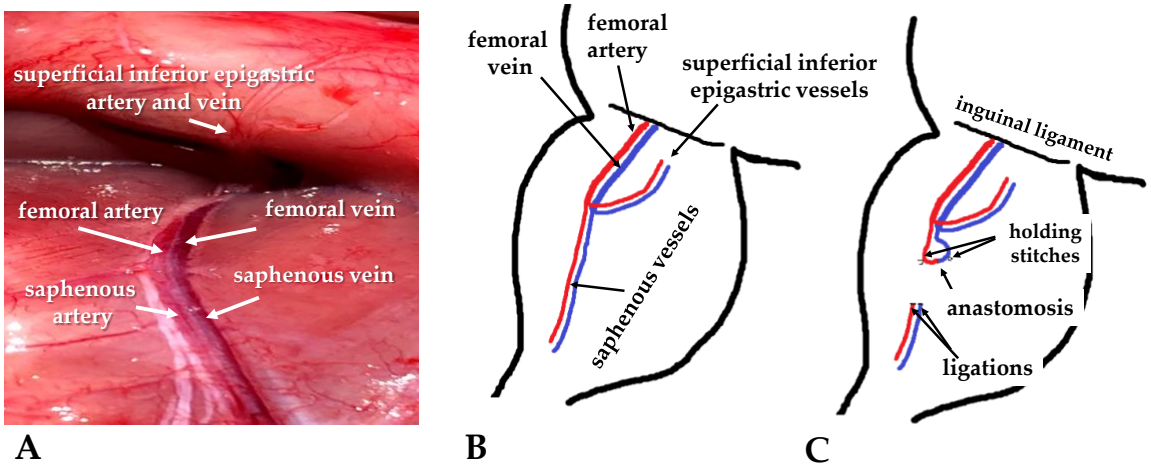


**Figure 5.**
Intraoperative photos of the intact vessels (**A**), schematic drawing of the affected vessels (**B**), and the localization of the anastomosis (**C**).

Their sizes ranged from 0.3 to 0.4 mm. Exact dissection was used to reveal the veins (Figure 6, A). Cutting the vascular was made easier by performing proximal and distal ligation of the vein and artery (Figure 6, B). The vein was cut farther than the artery to give room and flexibility for the next surgical steps (Figure 6, C). Heparin was used to clean the vessels, and they were then cautiously moved into their proper location (Figure 6, D).

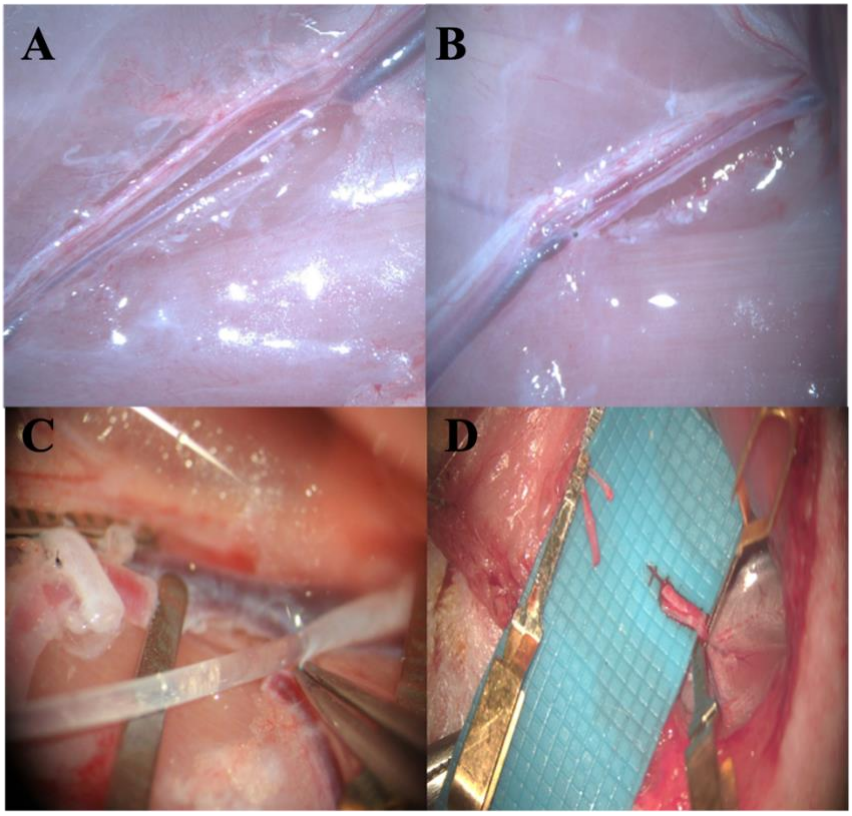


**Figure 6.**

Intraoperative view (captured from video recording) of complete dissection (**A**), proximal and distal ligation (**B**), heparin washing (**C**), cutting the vessels (**D**)

A successful end-to-end anastomosis was achieved by using three 3/8 serosa (taper) needles with 10/0 non-absorbable monofilament polyamide-6 sutures (Daclon, SMI, Saint Vith, Belgium) simultaneously. Because of the vessels' small dimensions and propensity to collapse, this method was found to be less stressful and time-efficient. Without knotting, the first needle was used to position the first suture in both vessels at the 12 o'clock position. After that, the identical procedure was carried out again, this time inserting the needle into the opposite end of the vessel at the six o'clock position, creating a wrapped shape. Midway between the first two entry locations was where the third needle was put next. The front wall of the anastomosis was sealed by tying and knotting the three threads after they had been secured. The vessels

were then turned over, and the anastomosis was completed by tying a fourth knot in the center of the back wall (Figure 7).

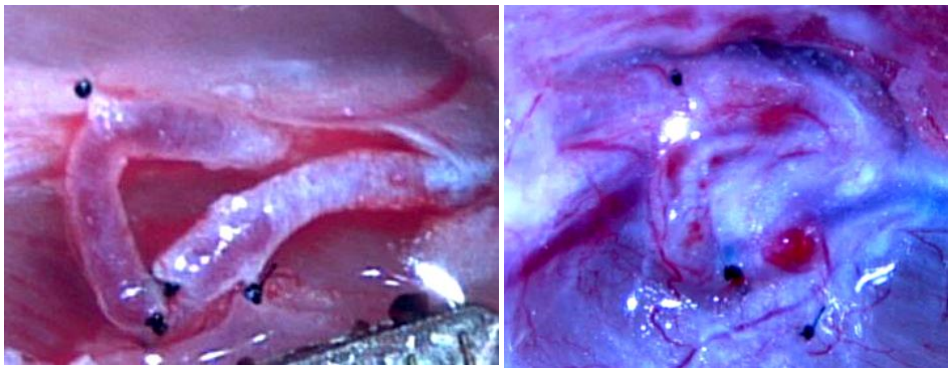

A B

**Figure 7.**
Intraoperative view (captured from video recording) of the freshly performed shunt (**A**), and the picture on the 12$^{th}$ postoperative week (**B**).

After the anastomosis was finished, we checked for flow leakage. Any defects in the anastomosis were noted when the proximal microvascular clip was taken out of the venous side. In order to improve coagulation, subcutaneous fat may need to be temporarily placed on the anastomosis after the arterial microvascular clip was removed if no issues were detected. Anastomosis patency was assessed using the twofold occlusion test or the milking test. In order to close the skin, a continuous suture with a 3/8 cutting needle and 5/0 absorbable polyglycolic acid thread was used.

The sham-operated group had an identical skin incision made after anesthesia, which was followed by dissection. The rats were sedated for sixty minutes, which is the same amount of time needed for the anastomosis in the AVM group to be finished. Similar to the AVM group, the sham-operated group's skin closure was carried out.

Tramadol (15 mg/bwkg, i.p.) was administered for analgesic during the first three postoperative days. Regular surveillance and wound care were conducted over the 12-week follow-up period.

### 4.3. Ultrasound examination

On the third, seventh, and twelfth postoperative weeks, echocardiography was carried out using a high-frequency transducer (MX250, 14–28 MHz) connected to a Vevo 3100 Ultrasound Imaging System (Fujifilm VisualSonics Inc., Toronto, ON, Canada). Rats were given an intraperitoneal ketamine-xylazine solution (50/5 mg/kg) to induce anaesthesia. After

shaving, the rats were put onto a VisualSonics SR200 platform, which monitors HR and the ECG in real time.

The American Society of Echocardiography's guidelines for evaluating cardiac function were followed. The following views were used in the construction of the database: B-, 2D-, M, Doppler modes; parasternal long and short axis; suprasternal (aortic arch); and apical four-chamber views (PSLAX, PSAX, SST, and A4C, respectively), B-, 2D-, M-, and Doppler modes. Using the VevoLAB programme (version 5.1, Fujifilm VisualSonics Inc., Toronto, ON, Canada), a blinded reader examined data offline after acquisitions. The recorded ECG's R-R intervals during a 5-second period were automatically used to compute heart rate.

At the midpoint of the papillary muscles, wall thickness and chamber sizes were determined in M-mode using PSLAX and PSAX views. M-mode pictures were also used to calculate the maximal diameter of the left atrium (LA) in millimeters and the diameter of the aortic root (Ao) in millimeters. M-mode tracing in PSLAX view was used to assess the left ventricle's internal diameter in end-diastole (LVIDd, mm) and end-systole (LVIDs, mm), as well as the anterior and posterior LV wall thickness (mm, LVAWd, LVAWs, and LVPWd, LVPWs, respectively).

The software computed the left ventricular volume in end-diastole and end-systole (LVVOLd, LVVOLs, respectively; µL). The formula for calculating the left ventricular ejection fraction (LVEF,%) was 100*(LVVOLd-LVVOLs)/LVVOLd. Automatic calculations were made using SV*HR for cardiac output (CO, mL/min) and LVIDd-LVIDs for stroke volume (SV, L).

Pulsed-wave Doppler (PW) and tissue Doppler imaging (TDI) from apical four-chamber views were used to assess diastolic function. PW Doppler echocardiography was utilised to calculate the E wave deceleration time (DecT, ms) and the ratio of the transmitral early (E) and atrial (A) peak flow velocities (E/A ratio). Using PW Doppler imaging in the left ventricular cavity, four parameters were measured: left ventricular ejection time (LVET, ms), isovolumic contraction time (IVCT, ms), isovolumic relaxation time (IVRT, ms), and c (MCOT, ms).

The formula used to calculate the cardiac performance index (MPI) was (MCOT-LVET)/LVET. Additionally, aortic flow (Ao) characteristics were evaluated using the modified suprasternal view in the PW Doppler mode. The programme was used to manually trace the boundaries of the Doppler jet before measuring the aorta velocity time integral (Ao VTI, mm), pressure gradients (Ao mean Grad, Ao peak Grad, mmHg), and aortic flow velocities (Ao mean Vel, Ao peak Vel, mm/s).

A modified PSLAX image was used to see the pulmonary vein [53]. Measurements included pulmonary vein atrial reversal peak velocity (PV Ar, mm/s) and duration (PV ARdur, ms), as well as systolic and diastolic deflections (PV S, mm/s and PV D, mm/s). At the septal annulus, tissue Doppler imaging (TDI) was used to assess peak tissue velocities at systole (s', mm/s), as well as in early (e', mm/s) and late (a', mm/s) filling. The ratio of e' to a' was used to define wall motion velocity. Additionally, the E/e' ratio was established. Every metric was averaged over three cardiac cycles, and the results are shown as the mean ± S.D.

### 4.4. Hemodynamic measurements

In our study, we conducted hemodynamic measurements encompassing systolic and diastolic blood pressure and heart rate. For the twelve-week follow-up, we utilized an invasive approach, inserting a catheter into the left femoral artery. The equipment used was the LD-01 system from Experimetria Ltd., Hungary, with a G20 cannula serving as the catheter. This system allowed us to measure SBP, DBP, and heart HR. During the invasive measurements, we analyzed data spanning 10 seconds for each case. The average of the highest pressure readings was taken as the SBP value, while the average of the lowest pressure readings was used to determine the DBP value. Additionally, the HR value was calculated as the average of seven measured HR values. After the hemodynamic measurements, the animals were over anesthetized.

### 4.5. Blood sampling protocol

First, third, fifth, seventh, ninth, and twelfth postoperative weeks (PO1, PO3, PO5, PO7, PO9, and PO12) were among the times when blood samples were taken from the tail cannula (Figure 8), in addition to both before and after the procedure. For hematological and hemorheological measures, 300 µl of the collected blood was obtained each time and deposited in Vacutainer tubes (BD Vacutainer® tubes, 5.4 g K3-EDTA, 3 ml). The rats underwent further postoperative weeks whereby the lateral tail vein was cannulated for the purpose of taking samples after they were sedated using the same anesthetic combination.

**Figure 8.**
Puncturing the lateral teil vein and inserting a 26-G cannula for blood samplings.

### 4.6. Hematological measurements

Hematological parameters were analyzed using the A Sysmex K-4500 automate (TOA Medical Electronics Co., Ltd., Japan), as shown in Figure 8. This analysis requires approximately 70 µl of blood. The parameters evaluated included: white blood cell count (WBC [$10^9$/L]), red blood cell count (RBC [$10^{12}$/L]), hemoglobin concentration (Hgb [g/L]), hematocrit percentage (Hct [%]), mean corpuscular hemoglobin (MCH [pg]), mean corpuscular volume (MCV [fl, femtoliter]), mean corpuscular hemoglobin concentration (MCHC [g/dl]), red blood cell size distribution (RDW-CV%), platelet count (Plt [$10^9$/L]), and mean platelet volume (MPV [fl]).

### 4.7. Hemorheological measurements

The deformability of RBCs in our study was assessed using the laser diffraction ektacytometry technique. This method enables the measurement of RBC elongation under specific shear stress through laser diffraction patterns (151).

We use the LoRRca MaxSis Osmoscan, a device produced by Mechatronics BV in the Netherlands, also known as Lorrca® (Laser Optical Rotational Red Cell Analyzer). The test requires a highly diluted blood sample: 10 µl of blood is mixed with 2 ml of PVP in PBS, having a viscosity of 27 mPas, osmolarity of 300 mOsm/kg, and pH of approximately 7.3. RBCs are subjected to increasing levels of SS, and their elongation is measured across a range of shear stresses from 0.3 to 30 Pa. The results are depicted as EI-SS (elongation index - shear stress) curves (Figure 9) (152).

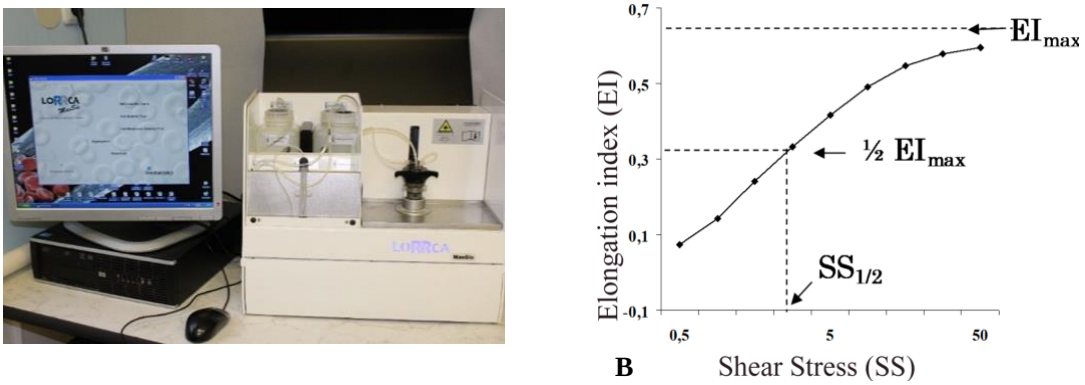


**Figure 9.**
The LoRRca MaxSis Osmoscan ektacytometer used to measure the deformability (**A**), and the principle of ektacytometry method (**B**)
(source: photo and figure collection of the Department of Operative Techniques and Surgical Research)

An individual curve represents each sample, and comparisons between cases are made by analyzing these curves. We assess these curves using parameters such as the $EI_{max}$, the shear stress at half of the maximum elongation index ($SS_{1/2}$ [Pa]), and the ratio of $EI_{max}$ to $SS_{1/2}$. These parameters are determined through Lineweaver-Burke analysis, using the formula: $1/EI = (SS_{1/2}/ EI_{max}) \times (1/SS) + (1/EI_{max})$ (Figure 9B) (153,154).

During the follow-up period, we studied RBC aggregation and RBC deformability. A Myrenne MA-1 erythrocyte aggregometer device (Myrenne GmbH, Germany) uses the light-transmittance method to express the aggregation index values in order to measure erythrocyte aggregation. The M1 5s and M1 10s aggregation indices were determined at a shear rate of 3 $s^{-1}$, and M 5s and M 10s were examined at a share rate of 0 $s^{-1}$.

### 4.8. Histological investigation

The heart and blood vessels were among the histology samples that were dissected under an operating microscope and preserved for a week in 4% formalin. The samples were embedded and sectioned (5 µm thickness) after fixation. The sections were then stained with H&E. The morphology of the heart was next examined using a Ventana DP200 scanner (Hoffman-La Roche, Roche Holding AG, Basel, Switzerland) in order to look for any structural or morphological variations between the two groups' cardiomyocytes and blood vessels.

Three different parts of the heart were measured: the basal, middle, and apex, to guarantee a comprehensive inspection of the histology slides. In this study, there were two groups: the control group (which included eight healthy hearts and twelve intact saphenous

vessels) and the AVM group (which had eight hearts, twelve intact saphenous arteries, and eight anastomosed saphenous vessels).

Each animal's heart had its left ventricle's wall diameter measured, and each section's 100 cardiomyocytes were evaluated, yielding 12 wall diameters and 300 cardiomyocytes for each animal's heart. These measurements were made at several points around the left ventricle. The cells were viewed horizontally, and their diameters were measured after zooming in.

Both the control and AVM groups removed saphenous vessels from the left non-operated leg and the right operated leg in addition to the heart analysis. The AVM group also performed an examination of the anastomosis location. The control group also had saphenous vessels taken from both legs. Samples of vessels were dissected in conjunction with the surrounding tissue in order to maintain their geometry. Ten measurements were made for each of the three layers—tunica externa, tunica media, and tunica intima—in each vessel. As a result, each histology slide had a total of thirty measurements.

With the aid of the 3DHistech Slide Viewer programme, which allowed for exact measurements, the histology slides of the hearts and blood arteries were assessed. The outcome's data were entered into an Excel document and thereafter examined.

### 4.9. Statistical analysis

The sample size was ascertained by applying Mead's resource equation approach. The significance level was chosen at $p < 0.05$, and the statistical analysis was performed utilizing GraphPad Prism 10 software. All data distributions had their normalcy examined. ANOVA tests in both directions, non-parametric tests like Wilcoxon or Mann-Whitney, and the Student t-test were used, depending on the findings. Also, for intra-group comparison Kruskal-Wallis and Dunn’s method of ANOVA tests were applied.

## 5. RESULTS

### 5.1. Echocardiography

Preoperative and the third, seventh, and twelfth postoperative weeks were used for LV ultrasound evaluations. A sample of the recordings from both groups is shown in Figure 10.

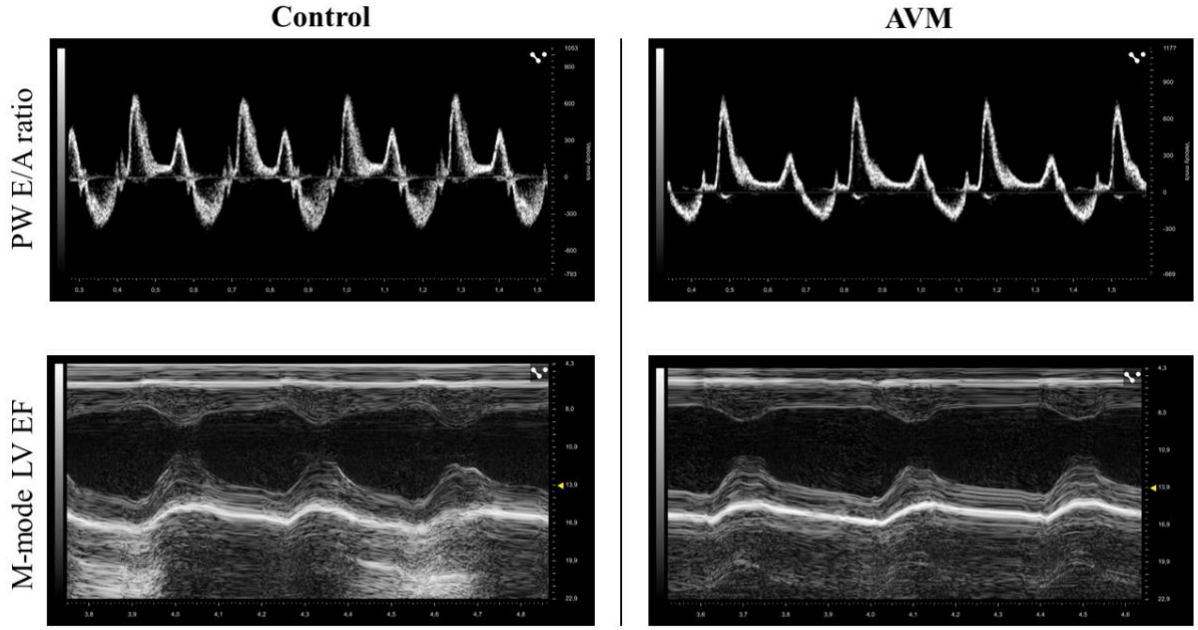


**Figure 10.**
Illustrative echocardiographic recordings from both the control and AVM study groups.

In terms of the posterior wall's thickness during systole, the control group showed an initial decrease from 3.43 ± 0.41 mm to 3.13 ± 0.51 mm, then a rise to 3.57 ± 0.54 mm, followed by a drop to 3.24 ± 0.55 mm. The AVM group followed a similar trajectory, initially decreasing from 3.57 ± 0.54 mm to 3.33 ± 0.68 mm, then increasing to 3.46 ± 0.67 mm, and eventually decreasing to 3.09 ± 0.39 mm (as shown in Figure 11, A). Regarding the posterior wall's thickness during diastole, it remained relatively consistent throughout the duration of the study for both control and AVM groups (as depicted in Figure 11, B).

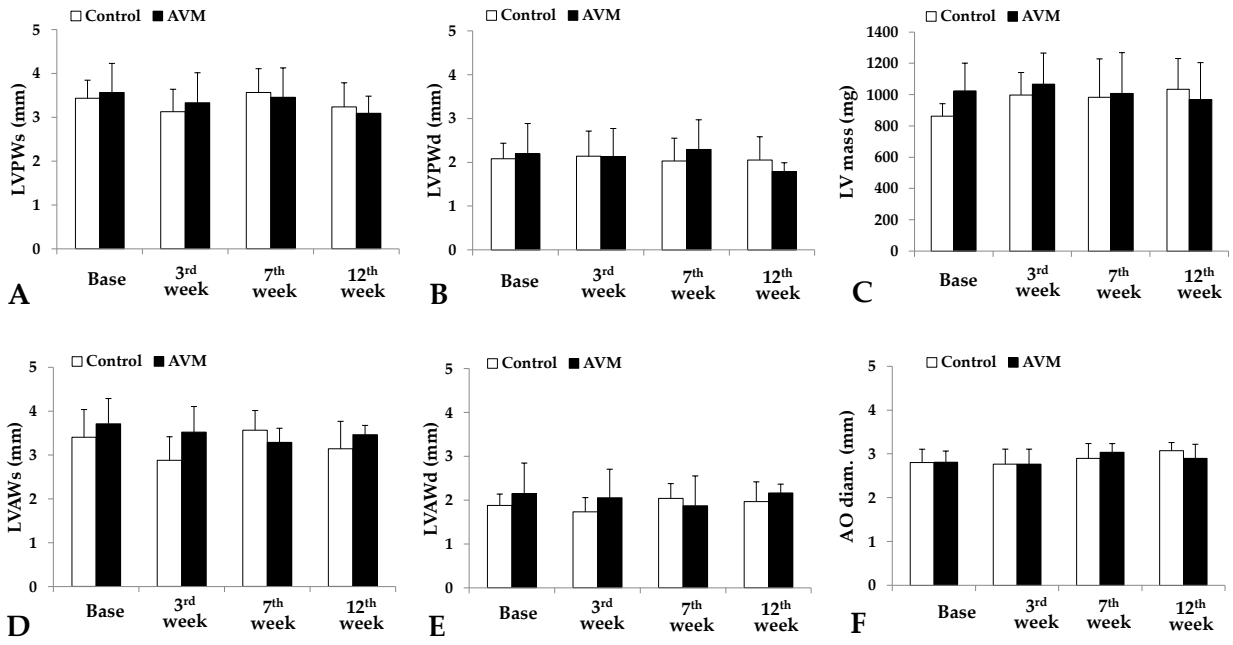


**Figure 11.**
Echocardiography data gathered pre-operatively and during the 3rd, 7th, and 12th postoperative weeks, detailing: systolic thickness of the left ventricular posterior wall (LVPWs [mm]) (**A**), diastolic thickness of the left ventricular posterior wall (LVPWd [mm]) (**B**), left ventricular mass (LV mass [mg]) (**C**), systolic thickness of the left ventricular anterior wall (LVAWs [mm]) (**D**), diastolic thickness of the left ventricular anterior wall (LVAWd [mm]) (**E**), and aortic diameter (AO diam. [mm]) (**F**).
Presented values are means ± standard deviation (S.D.).

During systole, the anterior wall thickness in the control group showed a reduction in the 3rd postoperative week, followed by a return to initial values later in the study. In the AVM group, there was an initial decrease in anterior wall thickness from 3.72 ± 0.57 mm before surgery to 3.29 ± 0.32 mm in the 7th postoperative week, with an eventual increase to 3.47 ± 0.21 mm by the 12th week, as indicated in Figure 11, D. Regarding the diastolic thickness of the anterior wall, the control group experienced a thickness peak in the 7th postoperative week, followed by a decrease in the 12th week. On the other hand, the AVM group showed only slight changes, maintaining a relatively steady thickness of around 2 ± 0.13 mm (Figure 11, E). None of the observed changes in anterior and posterior wall thickness during both systole and diastole, whether comparing between groups or within the same group before surgery and during the follow-up period, demonstrated statistical significance.

In terms of LV mass, the control group saw a slight increase from 863.15 ± 78.7 mg before surgery to 997.8 ± 143.4 mg in the 3rd postoperative week, with values remaining fairly stable thereafter. The LV mass in the AVM group remained consistently around 1000 ± 41.1 mg throughout the follow-up period, as depicted in Figure 11, B. The aortic diameter exhibited

an increase in both groups as the animals aged, as shown in Figure 11, F. Additionally, both groups' body weight increased by the 12th postoperative week as the rats aged (control group: 18.56 ± 6.16%, AVM group: 16.56 ± 3.22%).

Heart rate in the control group experienced a slight rise from 217 ± 40.5 beats per minute ($min^{-1}$) before surgery to 231 ± 36.32 $min^{-1}$ in the 3rd week, followed by a decrease to 200.8 ± 14.68 $min^{-1}$ by the 12th week. Conversely, in the AVM group, the heart rate started at 255 ± 53.66 $min^{-1}$ and gradually declined significantly throughout the study to 164.2 ± 27.71 $min^{-1}$, as illustrated in Figure 12, A. These findings provide a comprehensive view of heart structure and function changes over time in both the control and AVM groups.

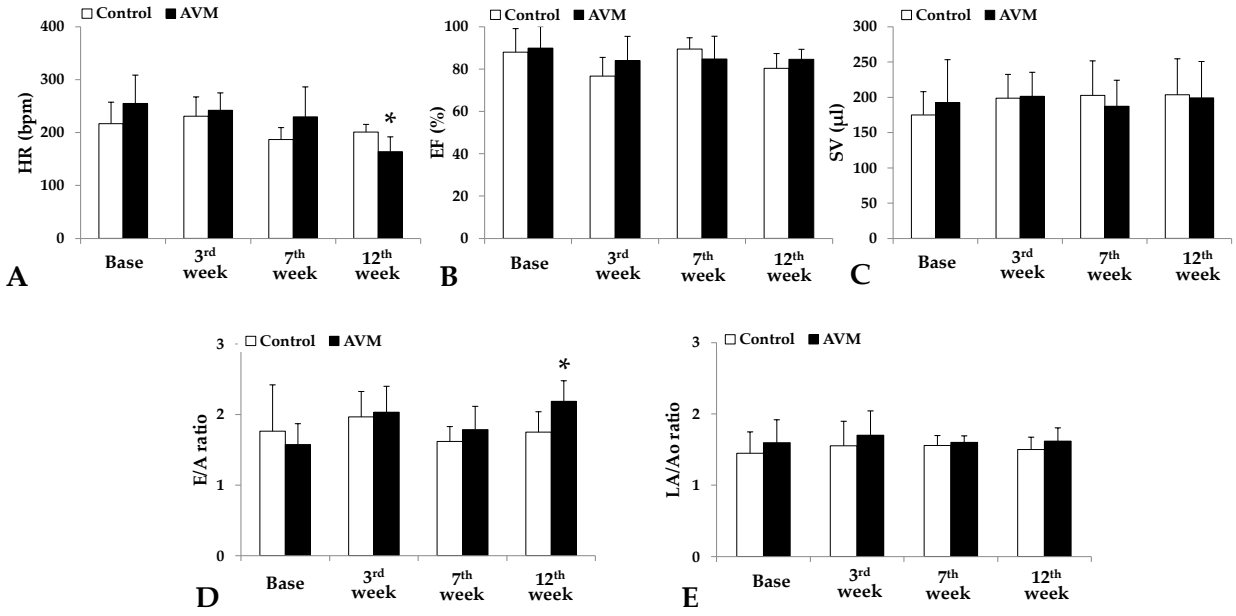


**Figure 12.**
Echocardiographic data captured preoperatively and at the 3rd, 7th, and 12th weeks post-surgery, showing: heart rate (HR [beats per minute, bpm]) (**A**), ejection fraction (EF [%]) (**B**), stroke volume (SV [µL]) (**C**), the ratio of early to atrial peak mitral inflow velocities (E/A ratio) (**D**), and the size of the left atrium relative to aortic diameter (LA/Ao ratio) (**E**).
means ± S.D., *p < 0.05 compared to baseline

Ejection fraction in the control group commenced at 88.03±11.1 %, experienced a 10-point drop in the 3rd week, peaked at 89.5±5.29 %, and subsequently declined to 80.4±6.93 %. In the AVM group, ejection fraction began at 89.85±10.21 % and decreased in the PO weeks to 84.09±11.37 %, 84.07±10.82 %, and 84.58±4.76 % (Figure 12, B).

Regarding stroke volume, the control group exhibited a steady increase from 175.2±32.8 µL, 198.7±33.77 µL to 202.6±48.91 µL, and to 203.5±51.6 µL. In contrast, the

AVM group initially increased from 192.4±60.83 µL to 201.5±33.94 µL, subsequently declined, and finally rose to 199.1±51.61 µL (Figure 12, C).

In the control group, the E/A ratio peaked at 1.97±0.36 in the 3rd week but dropped dramatically by the 7th week. By the end of the study period, it had returned to a normalized value of 1.75±0.29. The AVM group had varying values for this parameter during the follow-up period (Figure 12, D). Both groups exhibited minimal fluctuations in the LA/Ao ratio (Figure 12, E).

The peak gradient in the control group demonstrated minimal fluctuations. In contrast, the AVM group began at 2.7±0.84 mmHg, increased to 3.17±1.3 mmHg, experienced a slight decline to 2.93±1.02 mmHg, and finally peaked at 3.44 mmHg (Figure 13, A).

In terms of deceleration time, the control group peaked in the seventh postoperative week at 67.08±7.61 ms, but by the end of the study period, it had normalized to 54.5 ±7.54 ms. On the other hand, the AVM group experienced no notable changes during the third post-operative week, a minor increase in the seventh week, and a peak of 61.8 ±5.75 ms in the 12th week, following an initial value of 51.3 ±6.11 ms before to surgery (Figure 13, B). The AVM group had a substantial increase in aortic mean velocity (Figure 13, C).

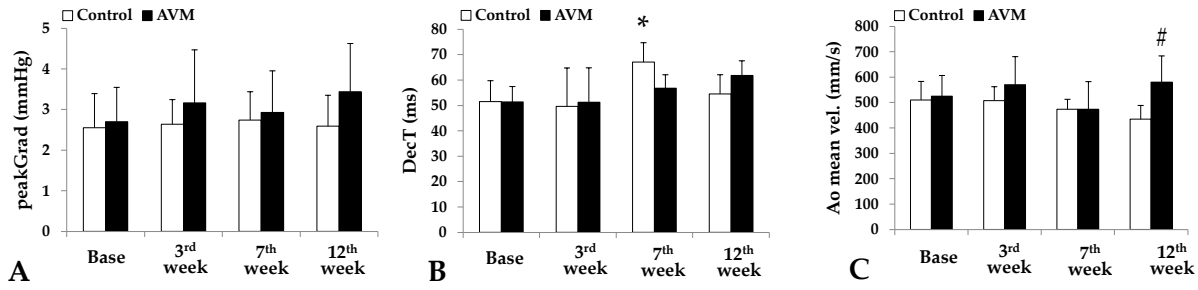


**Figure 13.**
Parameters obtained from the echocardiography recordings pre-operatively and on the 3rd, 7th and 12th postoperative weeks: peak gradient [mmHg]) (**A**), deceleration time (DecT [ms]) (**B**), and aortic mean velocity [mm/s] (**C**).
means±S.D. *p<0.05 vs. base. #p<0.05 vs. control

### 5.2. Weight and Hemodynamic parameters

Our findings revealed a minor decrease in the body weight of rats in the AVM group, possibly due to post-operative stress. However, rats regained and continued to gain weight during the 12-week follow-up. Both groups showed an increase in body weight over this period

(Control group: from 299.2±4.55g to 355±13.88g, an increase of 18.56±6.16%; AVM group: from 287.25±8.66g to 334.89 g, an increase of 16.56 ± 3.22%).

In the 12th week, prior to tissue sampling and extermination, tests on hemodynamic parameters (heart rate [bpm], systolic and diastolic blood pressure, and mean arterial pressure [mmHg]) did not reveal any significant differences (Table 3).

**Table 3.** Heart rate, systolic blood pressure, diastolic blood pressure, and mean arterial pressure measurements taken 12 weeks post-surgery in both the Control and AVM groups.

| Group | Heart rate [bpm] | Systolic blood pressure [mmHg] | Diastolic blood pressure [mmHg] | Mean arterial pressure [mmHg] |
|---|---|---|---|---|
| Control | 190.5 ± 16.87 | 111.74 ± 24.75 | 94.05 ± 15.2 | 99.95 ± 18.22 |
| AVM | 173.5 ± 41.86 | 105.65 ± 8.56 | 82.02 ± 2.77 | 89.9 ± 2.59 |

Means±S.D.

### 5.3. Hematological parameters

The majority of the noteworthy alterations in the haematological parameters were noted during the PO1, when the red blood cell count, hematocrit, and haemoglobin concentration levels significantly decreased in both groups (Table 4). Nonetheless, by the end of the PO12, these numbers returned to normal. When comparing the platelet count during PO5 to the preoperative status, the AVM group's was significantly greater than the control group's. Furthermore, even while both groups' leukocyte counts raised during surgery, the AVM group's leukocyte count continued to rise until the PO7. On the other hand, at the conclusion of the study period, the WBC count normalized in both groups (Table 4).

### 5.4. Hemorheological alterations

Figure 14 presents the cumulative EI and SS curves for both the Control and AVM groups. The EI values' standard deviation was minimal, resulting in curves that nearly coincided and exhibited no significant differences. Table 5 provides a comparative analysis of the EI-SS curves. In the AVM group, there was a minor, non-significant reduction in EI at 3 Pa by the first postoperative week, accompanied by a moderate rise in $SS_{1/2}$, leading to a lower $EI_{max}/SS_{1/2}$ ratio. Apart from these observations, the values between the two groups were largely comparable.

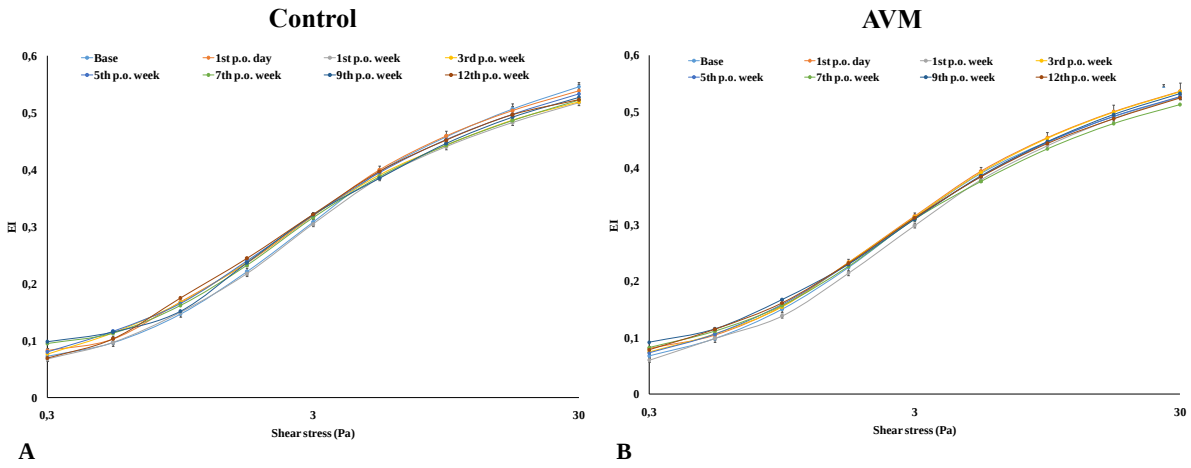


**Figure 14.**
Elongation index (EI) – shear stress (SS, Pa) curves of the Control (**A**) and AVM (**B**) groups during the follow-up period of 12 weeks.
Means ± S.D.

**Table 4.** Alterations of white blood cell count (WBC [$10^9$/L]), red blood cell count (RBC [$10^{12}$/L]), hematocrit (Hct [%]), hemoglobin concentration (Hbg [g/L]), mean corpuscular volume (MCV [fL]) and platelet count (Plt [$10^9$/L]) in Control and AVM group during the follow-up period of 12 weeks.

| Variable | Group | Base | 1st p.o. day | 1st p.o. week | 3rd p.o. week | 5th p.o. week | 7th p.o. week | 9th p.o. week | 12th p.o. week |
|---|---|---|---|---|---|---|---|---|---|
| WBC ($10^9$/L) | Control | 9.27±1.68 | 11.28±1.04 | 7.28±1.57 | 5.32±0.54 | 7.93±1.53 | 11.15±2.56 | 8.52±1.01 | 8.22±1.75 |
| | AVM | 10.53±1.18 | 13.19±1.73 | 10.96±1.19 | 11.49±1.48 | 8.59±1.93 | 22.01±9.98 | 6.69±1.43 | 10.02±1.44 |
| RBC ($10^{12}$/L) | Control | 6.86±0.51 | 6.56±0.59 | 5.45±0.8 | 6.6±0.31 | 6.4±0.65 | 7.12±0.61 | 6.47±0.31 | 7.18±0.69 |
| | AVM | 7.1±0.57 | 6.57±0.37 | 6.71±0.52 | 7.28±0.53 | 6.85±0.62 | 7.49±0.28 | 6.86±0.81 | 7.28±0.3 |
| Hct (%) | Control | 39.52±2 | 36.5±2.1 | 29.31±1.31 | 39.07±1.79 | 36.45±2.83 | 40.68±2.84 | 36.6±1.53 | 39.79±3.14 |
| | AVM | 39.75±1.96 | 36.79±2.04 | 38.54±2.58 | 42.1±2.31 | 40.08±2.12 | 42.11±1.07 | 40.68±3.31 | 40.59±1.88 |
| Hbg (g/L) | Control | 137.1±5.91 | 126±10.64 | 101.9±6.64 | 133.1±5.48 | 126.41±11.62 | 136±8.7 | 124.5±7.72 | 138.25±10.01 |
| | AVM | 141.71±8.62 | 132±2.75 | 132.83±5.49 | 145.83±6.26 | 135.58±7.43 | 146.38±4.44 | 138.67±10.66 | 141.58±4.52 |
| MCV (fL) | Control | 56.53±0.96 | 55.45±0.99 | 56.25±1 | 58.61±0.96 | 56.96±0.93 | 56.71±0.77 | 56.55±0.37 | 56.91±0.48 |
| | AVM | 55.84±1.65 | 55.72±1.29 | 57.17±1.14 | 57.51±1.29 | 58.3±1.09 | 56.4±1.08 | 57±1.25 | 56.39±1.2 |
| Plt ($10^9$/L) | Control | 789.8±39.1 | 704.7±36.5 | 889.7±108 | 932.3±134.6 | 773.1±138.2 | 884.1±77.4 | 906.7±26.8 | 965.4±136.9 |
| | AVM | 833±62.7 | 707.3±124.7 | 975.5±147.3 | 783.6±104.1 | 791.2±83 | 938.2±35.7 | 792.7±147.3 | 922.9±77.1 |

means±S.D.

**Table 5.** Comparative parameters of RBC elongation index (EI) – shear stress (SS) curves in Control and AVM group during the 12-week follow-up period.

| Variable | Group | Base | 1st p.o. day | 1st p.o. week | 3rd p.o. week | 5th p.o. week | 7th p.o. week | 9th p.o. week | 12th p.o. week |
|---|---|---|---|---|---|---|---|---|---|
| EI at 3 Pa | Control | 0.308±0.056 | 0.319±0.041 | 0.304±0.047 | 0.319±0.037 | 0.319±0.042 | 0.315±0.041 | 0.318±0.039 | 0.321±0.041 |
| | AVM | 0.311±0.044 | 0.315±0.043 | 0.298±0.047 | 0.314±0.048 | 0.311±0.046 | 0.309±0.037 | 0.309±0.042 | 0,312±0.043 |
| $EI_{max}$ | Control | 0.576±0.027 | 0.589±0.028 | 0.583±0.053 | 0.563±0.046 | 0.573±0.024 | 0.565±0.027 | 0.566±0.018 | 0.571±0.035 |
| | AVM | 0.585±0.04 | 0.587±0.026 | 0.593±0.045 | 0.587±0.030 | 0.578±0.031 | 0.548±0.051 | 0.582±0.032 | 0.568±0.026 |
| $SS_{1/2}$ (Pa) | Control | 2.82±1.25 | 2.71±1 | 3.11±1.41 | 2.52±1.07 | 2.51±0.91 | 2.58±0-96 | 2.5±0.36 | 2.51±1.11 |
| | AVM | 2.93±1.22 | 2.78±1.14 | 3.32±1.54 | 2.85±1.23 | 2.83±1.27 | 2.84±1.23 | 2.87±1.25 | 2.64±1.01 |
| $EI_{max}/SS_{1/2}$ ($Pa^{-1}$) | Control | 0.222±0.102 | 0.244±0.08 | 0.222±0.09 | 0.258±0.096 | 0.244±0.085 | 0.244±0.082 | 0.252±0.091 | 0.271±0.115 |
| | AVM | 0.229±0.082 | 0.242±0.084 | 0.216±0.092 | 0.243±0.096 | 0.245±0.09 | 0.229±0.09 | 0.238±0.094 | 0.245±0.089 |

means±S.D.

Figure 15 illustrates the variations in RBC aggregation indices throughout the study period. Observations of indices such as M 5s, M1 5s, M 10s, and M1 10s showed inconsistent changes over time, marked by fluctuations and broad individual differences, leading to significant data variance. In the AVM group, these values often saw an increase, remaining high until the 9th postoperative week, yet these variations were not statistically significant.

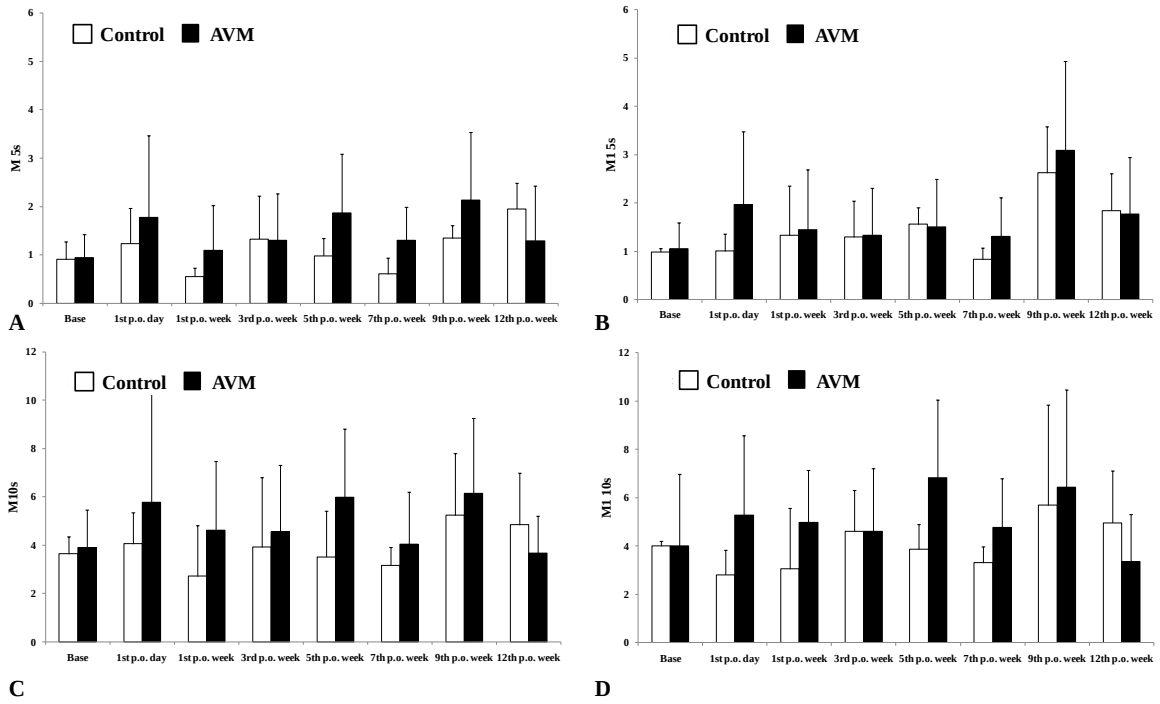


**Figure 15.**
Alteration of red blood cell aggregation index values:
M 5s (**A**), M1 5s (**B**), M 10s (**C**), and M1 10s (**D**).
Means±S.D.

## 5.5. Morphology of the shunts

Table 6 provides an overview of the vessel diameters. Only the arterial side of the fistula showed a significant difference (p=0.011 vs. preoperative condition, p=0.025 vs. control side) by the 12$^{th}$ postoperative week, despite a noticeable increase in both the venous and arterial branches.

**Table 6.** Measurements of the outer diameter [mm] of the saphenous artery and vein, recorded both before the surgery and 12 weeks post-operation.

| Localization | Artery [mm] | Vein [mm] |
|---|---|---|
| Control side preoperatively | 0.37 ± 0.02 | 0.37 ± 0.05 |
| Control side on the 12th p.o. week | 0.39 ± 0.05 | 0.41 ± 0.11 |
| Operated side preoperatively | 0.37 ± 0.03 | 0.38 ± 0.04 |
| Operated side on the 12th p.o. week | 0.49 ± 0.06 *# | 0.51 ± 0.1 |

Means±S.D., *p<0.05 vs. preoperative condition #p<0.05 vs. control side

## 5.6. Histomorphology

At the end of the 12-week observation period, the heart wall and myocyte thicknesses in the basal, middle, and apical incision planes showed comparable changes, which were most effectively represented by their combined average. With respect to wall thickness, there was a notable divergence between the AVM and control groups (p=0.0057). In the AVM group, there was a significant rise in the average myocyte thickness (p=0.0001), as seen in Figure 16, A.

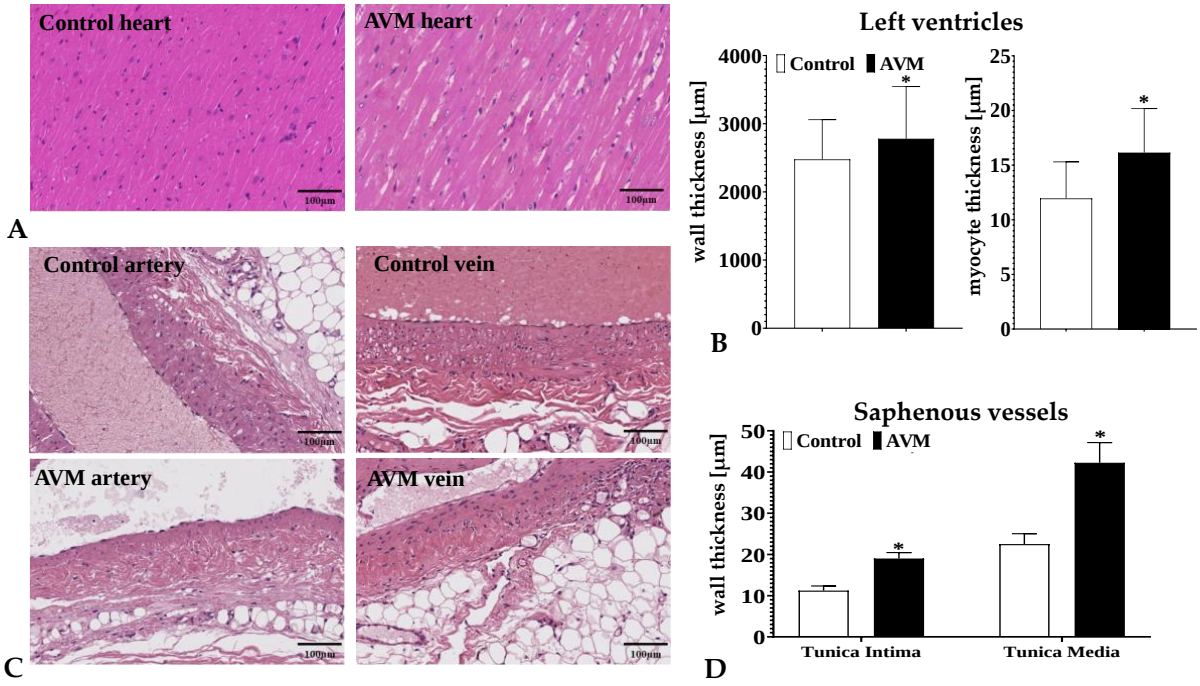


**Figure 16.**
Illustrative histological images stained with Hematoxylin and Eosin (H&E) of the left ventricle (**A**) and the saphenous vessels (**C**) from samples collected in the 12th postoperative week, along with the measurements of the left ventricle wall thickness (**B**) and the thickness of the vessel wall layers (**D**). Presented with H&E staining.
Data shown as means ± standard deviation (S.D.). * indicates p < 0.05 compared to the Control group.

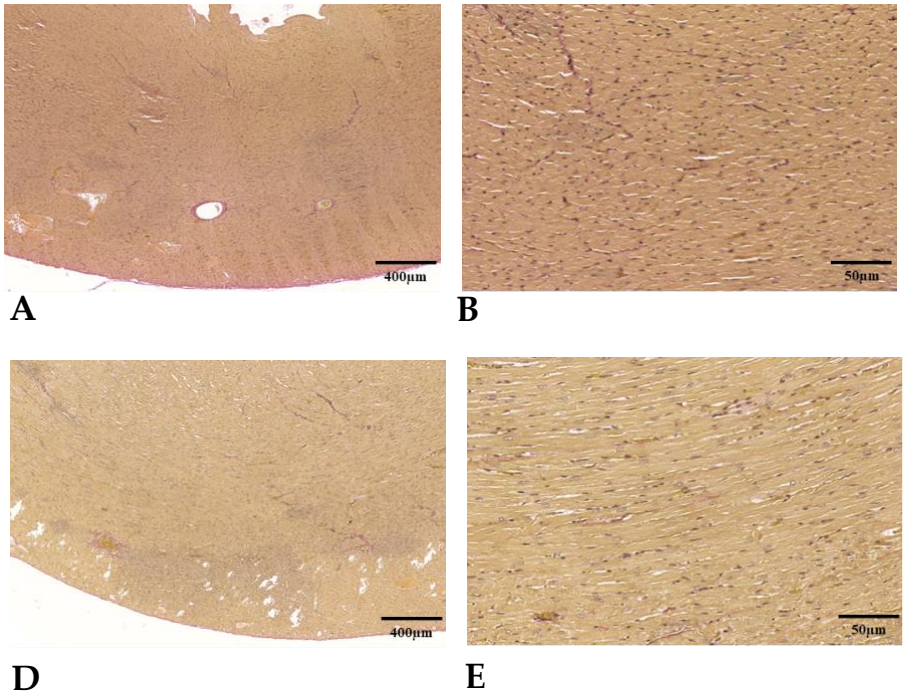


**Figure 17.**
Illustrative histological images of the left ventricle stained with Van Gieson, showcasing samples from the Control group (A,B) and the AVM group (C,D).

In none of the groups did the qualitative evaluation show any signs of cardiac fibrosis (Figure 17) resulting from microvascular ischemia or subsequent cellular death. Cardiomyocytes in the AVM group were notably hypertrophic, with abundant eosinophilic cytoplasm, nuclei that resembled boxes, and occasionally unusual forms like Y-shaped branching. Myocardial disarray was evident in the architectural arrangement of the myocardium, where cardiomyocyte bundles were placed at perpendicular and oblique angles. When compared to the control saphenous veins, the tunica intima and media layers of the saphenous vein at the anastomosis location dramatically enlarged (Figure 16, B).

## 6. DISCUSSION

In the initial phase, the research involved inducing hypoperfusion and venous hypertension in either the entire brain or specific regions using extra- or intracranial arteriovenous fistulae. This was done to assess hemodynamic and pathophysiological shifts in brain tissue near AVMs, both in the presence of AVMs and post-resection, aiming to elucidate symptomatology and reduce postoperative risks. Identifying unique vascular configurations, such as the rete mirabile in artiodactyls and the venous plexus in rats, facilitated the application of occlusive therapies (endovascular embolization, radiotherapy) and the evaluation of their efficacy. Subsequently, the genetic manipulation of angiogenesis pathways enabled the development of mutant mice models with authentic AVMs in the brain, enhancing the understanding of AVM genesis, evolution, and rupture. Innovative models, like those simulating AVM-like lesions in canine brains and grafting transgenic arteriovenous fistulae from mice to rats, contributed uniquely to exploring pathogenesis and new treatments. The rat cornea model mainly aided in examining angiogenic mechanisms in human AVM specimens.

A comprehensive AVM model replicating human AVMs' anatomical, physiological, biological, and clinical characteristics has yet to exist. Even the transgenic mice model, though featuring spontaneous systemic vascular malformations, fails to fully mimic the sporadic nature predominantly observed in clinical settings. Despite these constraints, these diverse models have been instrumental in addressing specific research queries in AVM studies.

AVM is challenging to emulate surgically due to the intricate nidus linking arteries and veins. Nevertheless, approximating its physiological aspects is feasible by constructing conditions akin to AVMs, particularly using vessels of similar diameter. This approach enables the examination of hematology and hemorheology in the anastomosis, correlating it with AVMs. Surgical vascular anastomosis typically involves side-to-end, end-to-end, or end-to-side configurations. In model construction, anastomosis is not restricted to suture methods or peripheral vessels; many models utilize central AVFs employing alternative techniques. This choice is influenced by factors like the small size of peripheral vessels and the meticulous effort required for microscopic suturing. One such method is the puncture technique, where adjacent vessels are pierced to form a channel, maintained open by arterial-venous pressure differences (155). Other documented techniques include arterial insertion into veins, the cuff technique, and various anastomosis forms (156–160).

For our study, we selected the suturing technique to create anastomoses between the relatively small peripheral saphenous vessels, aiming for long-term observation with minimal

complications. The two pivotal principles for anastomosis under microscopy are ensuring no tension on the anastomosis line and maintaining a moist working environment.

Certain tips can minimize frustration and time during surgery. Initially, it's essential to determine the correct incision site. Draw an imaginary line from the medial inguinal ligament to the knee joint; appropriate skin shaving reveals the saphenous vessels where the incision should be made in the mid-point. However, it's crucial to recognize that the saphenous vessels typically emerge after the epigastric vessels' origin. To avoid misidentification, atraumatic dissection should be used to trace these vessels precisely and carefully.

Once the vessels are located, check for any small muscular branches emanating directly from them. If present, either cut distally to these branches or ligate them. Planning subsequent steps is vital, particularly in deciding the anastomosis location. This decision should consider not only the vessels but also the workspace relative to surrounding structures. For example, cutting the saphenous vessel on its proximal half could restrict working space, complicating the procedure and extending its duration. Therefore, we recommend a distal cut on the saphenous vessel. Given that the saphenous vein and artery run parallel, and the goal is a U-shaped anastomosis, it's advisable to cut the artery more distally than the vein. This positioning facilitates an easier end-to-end anastomosis with the vessels facing each other.

Anastomosing such small vessels is a complex task that requires thorough training and patience. If difficulties arise, particularly with vessel collapse after the initial suture placement, a technique involving multiple needles simultaneously can be beneficial. This method avoids finalizing knots immediately. Begin by using one needle to create the distal corner suture, leaving it untied initially while maintaining thread tension. Follow this with a second needle to secure the proximal corner. Again, do not tie a knot initially, but apply tension on the thread opposite to the first needle's direction. Then, use a third needle for the mid-section suture.

Once all three needles/threads are correctly positioned, proceed to knot them in sequence: the distal, the proximal, the middle. Keeping the long ends of the thread on the proximal and distal sutures can assist in flipping the vessels for the back wall knot. This staged approach helps manage the procedure's delicacy and ensures the anastomosis's stability.

In our studies, the number of animals used was restricted in adherence to animal protection laws, limiting our ability to statistically analyze surgical complications occurring in individual cases. Nonetheless, documenting these complications is crucial for refining laboratory methodologies. Despite precautions and the clear surgical steps in our study, we had to practice for more than three months to complete the anastomosis, which helped us form the earlier described surgical protocol.

Reported mortality rates in similar studies vary widely, ranging from 0 to 47% (161–164). Higher mortality is often associated with central arteriovenous fistulas, where surgical trauma and risks of bleeding and infection are elevated. In these studies, most deaths occurred within 24-48 hours post-surgery, primarily due to congestive heart failure or other unidentified causes (161,162,165).

Our study, fortunately, did not witness any other surgical complications. There were no instances of postoperative death or wound-healing disorders. However, other studies have noted different complications. For instance, Langer et al. reported a case of septic thrombosis of the femoral fistula postoperatively (164).

It is acknowledged that every animal model has its pros and cons, and ours is no exception. While the puncture technique for creating fistulas is simpler and quicker than suturing, it is not viable in our case since we want to simulate a real AVM. Although other study methods may reduce surgical duration and trauma, our priority was performing safe anastomoses, with most surgical interventions in our study completed in under 60 minutes.

Simulating AVM hemodynamics is crucial for understanding its pathophysiology and enhancing endovascular treatment methods. Typically, models comprise an arteriovenous shunt and a nidus.

The swine rete mirabile, with its network of interconnected micro arteries resembling an AVM nidus angiographically, has been a model of choice (125). Yet, its arterial structure differs from the arterial-to-venous nature of human AVMs (125). A temporary arteriovenous shunt was established between the rete, the internal carotid artery, and the cavernous sinus to overcome this. Despite its structural similarity to human AVMs, this model causes several side effects in animals, such as proptosis and sub-conjunctival hemorrhage. It remains viable for about a week before spontaneous occlusion. While not located in the brain, this model is invaluable for refining endovascular techniques and testing new embolic materials (125).

Massoud et al. sought a simpler model by creating an AVM in the neck of swine, thereby avoiding the complications of the rete-cavernous fistula model. Three neck arteries are occluded to augment blood flow in the fistula, followed by a side-to-side carotid-jugular anastomosis (127).

Critiques of this model highlight the costly use of microcatheters and detachable balloons (122). Alternatively, Qian et al. developed a similar model in sheep without occluding arterial branches. The sheep's rete mirabile, differing structurally from swine's, presents as two units linked by bridging vessels, unlike the singular unit in swine. This distinction offers an advantage in sheep, allowing the study of multiple AVMs (122).

Swine are favored in research due to their large neck vessels, facilitating quicker and simpler fistula creation. Some models do not require occlusion of external arteries (166,167). Using end-to-end anastomosis rather than side-to-side has increased blood flow in the rete mirabile. Unlike previous models, these do not spontaneously occlude, making them suitable for longer-term research (125,127,166,167). The swine model also offers advantages like a coagulation system akin to humans and cost-effectiveness (127).

Hemodynamic models are crucial for investigating aspects such as perfusion pressure breakthrough, venous hypertension, and thrombosis in AVMs. Rats are commonly used for these studies (32,33). These models typically involve an anastomosis between the common carotid artery and the external jugular vein in the neck region (35,39,45,46). Here, the common carotid artery serves as the feeding artery, and the external jugular vein becomes the arterialized vein. For instance, one model connects the rostral carotid artery to the caudal jugular vein, leading to intracranial hypoperfusion similar to the "steal" phenomenon in AVMs, which is useful for studying chronic ischemia effects (31,34).

One of the earliest models using CJF for studying AVMs, was initially introduced by Spetzler and colleagues (40,168). Their work focused on examining the NPPB theory, which is associated with swelling and hemorrhaging in brain tissue surrounding AVM lesions after surgical intervention (169). Developed in cats, this model involved creating an anastomosis between the common carotid artery CCA and EJV. The purpose of this anastomosis was to induce non-infarction cerebral hypoperfusion by reversing blood flow from the circle of Willis (169). Despite its innovative approach, subsequent research reported only minimal and temporary changes in cerebrovascular hemodynamics following CJF formation (170,171), casting doubts on the model's effectiveness in fully exploring the underlying mechanisms of NPPB.

Morgan et al.'s carotid jugular fistula model, which involved an end-to-end anastomosis between the common carotid artery and the external jugular vein, was specifically employed to study hypoperfusion. This model's integration of intracranial arterial and venous systems with extracranial venous systems is a notable characteristic (31). Moreover, Morgan and his team developed an altered CJF model in rats, involving an end-to-end anastomosis of the rostral ends of both CCA and EJV. This model demonstrated a notable decrease in cerebral blood flow (CBF) on the side of the fistula over a period of 8-12 weeks. Sealing the fistula resulted in a significant increase in CBF, leading to the breakdown of the blood-brain barrier in hypertensive conditions (121,172). Rats were selected for this model primarily due to their cost-effectiveness and availability despite their anatomical variances from humans. Efforts

have been made to replicate CJF models in monkeys, but these are fraught with challenges related to management, high costs, and complex ethical issues (119).

In some models, the anastomosis involves a side-to-end connection between the common carotid artery and the rostral external jugular vein. In this configuration, arterial blood is directed through the external jugular vein and its branches, functioning as the "nidus". The blood then exits through the transverse sinus and the contralateral jugular vein, which acts as the draining vein (36,37). This model has been instrumental in exploring the molecular and morphological alterations in AVMs following radiosurgery treatments (38,39). Notably, it generates an endothelial phenotype similar to that observed in human AVMs, vital for examining the varied endothelial responses to radiation across different phenotypes. Additionally, it has been observed that blood flow in this model increases over time, persisting at least up to 42 days post-surgery (39).

In many AVM models that purport to replicate human AVM blood flow, the location is typically extracranial rather than intracranial (123,127,173). To address this discrepancy, a novel AVM model was developed using beagle dogs (124). This model involved an end-to-end anastomosis between the superficial temporal artery and the middle cerebral artery, along with an end-to-side anastomosis between the superficial temporal artery and the dorsal sagittal sinus. Additionally, a muscle graft, nourished by the superficial temporal artery, was implanted in the brain's ischemic region. This setup was observed to exacerbate ischemia in the arteriovenous fistula area (124). A significant benefit of this model is its intracranial location, providing a closer approximation to human AVM conditions. However, this particular model has not been reported in subsequent research studies.

Numazawa et al. devised a model to investigate hypoperfusion and impaired $CO_2$ reactivity. In this model, a femoral vein graft was utilized to form an arteriovenous shunt between a cortical branch of the middle cerebral artery and the superior sagittal sinus. This carotid-jugular fistula model led to immediate hemodynamic changes throughout the brain, especially in the hemisphere where the fistula was located, yet it had minimal effect on the regional brain tissue. This setup effectively mimicked the hemodynamics observed in AVM patients, characterized by hypoperfusion and diminished $CO_2$ reactivity (174).

To investigate localized cerebral hypoperfusion more closely, a dog model incorporating an intracranial arteriovenous fistula was employed. Dogs were chosen due to their brain size, which eases surgical procedures, and their physiological and hemodynamic characteristics that closely resemble humans. In this model, a craniotomy was performed, followed by the creation of a fistula using a femoral venous graft. When the shunt was opened,

there was a marked reduction in cerebral blood flow in the MCA area, but this effect was not observed in other brain regions. Re-occluding the shunt led to a rapid return of regional cerebral blood flow to its initial levels within 15 minutes. Additionally, regional $CO_2$ reactivity significantly decreased when the shunt was opened. The localized hemodynamic shifts in this animal model closely paralleled those observed in human brain tissue near AVMs. However, the model was short-term and the procedure was relatively complex. While focusing on hemodynamic and pathophysiological changes in tissues adjacent to AVMs, extracranial and intracranial arteriovenous fistula models did not incorporate an actual AVM nidus.

The rete mirabile serves as an effective model for advancing endovascular techniques, primarily due to its arterio-arterial system, which does not necessitate surgery. However, for research focused on the pathophysiology and hemodynamic aspects of AVMs, an arterio-venous shunt is essential. While the swine model is applicable for such studies, the rat arteriovenous model offers advantages in terms of easier animal care and maintenance and is more cost-effective compared to swine and sheep models.

We aimed to develop an AVM model that avoids the immediate and substantial hemodynamic and cardiac changes seen in other arteriovenous shunt models with larger calibers. Working with rat saphenous vessels requires advanced microsurgical techniques, yet this model has the potential to replicate a small, asymptomatic AVM. This offers an opportunity to delve into the factors influencing AVM progression, enlargement, and destabilization.

AVMs, with their complex network of feeding arteries and draining veins, are known to cause a range of symptoms, sometimes leading to severe neurological complications, disabilities, or even death due to hemorrhage (52,175). Believed to form during embryonic development, with possible postnatal occurrences, the intricacies of AVM etiology are still being unraveled (1,18). Despite significant medical research and technology strides, managing AVMs remains challenging, largely due to a limited understanding of their behavior and response to medical interventions (14,117,176).

Therefore, there's a critical need for an effective AVM model that closely mirrors human AVMs in anatomical, physiological, biological, and clinical aspects to enhance our understanding of their pathogenesis, behavior, and treatment responses.

A major drawback of most arteriovenous shunt models is the immediate impact on hemodynamics and cardiac function following arterial and venous connections. These models fail to represent the 'silent', asymptomatic AVMs and cannot track their gradual enlargement and progression.

Our study findings indicated that in the AVM group, hematological and hemorheological parameters remained largely unchanged compared to the sham-operated control group. However, likely due to acute phase reactions, there was an increase in leukocyte count in the early postoperative phase. A slight decline in red blood cell count, hematocrit, and hemoglobin was also noted, a trend observed in the sham-operated group as well. Factors such as repeated anesthesia during follow-ups for sampling, immobilization, recovery, blood sampling, and surgical procedures (like skin incisions, tissue handling, suturing, and wound healing) in both groups could account for these variations. This includes the irregular, minor rise in RBC indices and the temporarily moderate reduction in RBC deformability (177–179).

The hemorheological changes were more pronounced and significant in other rat models employing artificial arteriovenous shunts in larger vessels. For instance, in the carotid-jugular shunt model, which is technically simpler than the recent saphenous AVM model, RBC deformability was notably compromised by the end of a 6-week observation period (180). Mechanical stability tests revealed significantly lower deformability under stress than the sham-operated group (46), indicating that this model may not be suitable for studying AVM progression due to its immediate and substantial hemodynamic and hemorheological effects. The carotid-jugular fistula model was originally intended to monitor shunt maturation, not as an AVM model.

In another rat model, the superficial inferior epigastric vein was used to create an arteriovenous connection in the femoral region. Here, hematocrit, red blood cell count, and hemoglobin levels significantly dropped by the first postoperative week, and RBC aggregation notably increased by the fifth week (47). In these cases, the underlying causes of micro-rheological disturbances include acute phase-related immune/inflammatory processes, changes in oxygenation levels (dependent on the caliber and extent of blood mixing), and altered shear stress at and near the shunt sites (178,179).

The cardiac echography results from our study could be partially attributed to the aging of the animals, as changes were also noted in sham-operated controls. Moderate yet progressive changes were observed in cases of slowly developing and enlarging AVMs. By the 12th postoperative week, significant histological changes were evident in heart samples. The thickening of the shunt vessels' walls was consistent with findings in other arteriovenous shunt models of varying locations and sizes (45,181). For example, carotid-jugular fistula models showed immediate hemodynamic alterations and significant left ventricular hypertrophy within six weeks (45). Similarly, arteriovenous fistulas with different geometries in the femoral region led to notable hemodynamic shifts after five weeks, with vessel histology showing uneven

thickening due to varying intraluminal pressure and wall shear stress. Asymmetric shear stress distribution correlated with spots of intima hyperplasia. These vascular wall changes are attributable to altered local blood flow and shearing forces, as supported by numerous studies (182).

Interestingly, the changes observed were neither uniform nor continuously progressive across all parameters. Adaptation mechanisms in hemodynamics and cardiovascular function, along with the animals' aging and growth, might play a role. Though not apparent, differences in movement between non-operated and operated legs could also contribute to these complex changes.

AVF models have demonstrated a consistent increase in heart and lung weights proportional to the fistula's diameter (157,162,183–185). The impact of arteriovenous fistulas on body weight varies and is influenced by the fistula size and the post-surgery follow-up duration. Rapid weight gain post-surgery often indicates fluid retention. Some studies suggest that an increase of 50 grams or more within seven days is indicative of severe heart failure (185).

Our results align with other studies showing a temporary post-surgery weight decrease followed by normal weight gain, with no significant difference from the control group after a month (162,186).

Unlike other models, the arteriovenous fistula in this study did not result in significant left ventricular hypertrophy compared to the control group. This, combined with the high survival rate and lack of evident cardiac pathology, suggests that using saphenous vessels effectively avoids systemic circulatory effects.

The examination of H&E and Van Gieson stained sections showed no evidence of myocardial fibrosis due to microvascular ischemia or resultant cellular death in any group. In the AVM group, the cardiomyocytes displayed significant hypertrophy, characterized by abundant eosinophilic cytoplasm, square-shaped nuclei, and at times, unusual shapes like Y-shaped branching. The structural organization of the myocardium was disrupted, as observed by the disordered arrangement of cardiomyocyte bundles, positioned perpendicularly and obliquely to each other, suggesting myocardial disarray.

An additional observation was intimal hyperplasia in the venous limb of the fistula in the operated group, as opposed to the non-operated vein in the sham group, which was supported as well by the diameter of the operated artery and vein compared to the control group at the $12^{th}$ week post-operatively. The diameter of the operated arteries at $12^{th}$ post-operative week were significantly larger than the diameter of the same arteries pre-operatively and compared

to the control group at 12$^{th}$ week post-operatively. This model is therefore recommendable for studies investigating the rheology and hematology of AVMs, which can contribute to predicting AVM behavior.

Observing the systemic circulation and cardiac changes in carotid jugular fistula cases, we found contrasting results in our saphenous AVM model. Unlike the former studies, where significant alterations were evident after 6 weeks, in our study the rats were followed up for 12 weeks, and we observed no notable impact on systolic or diastolic function. In contrast to the structural changes seen in the left ventricle and reductions in ejection fraction and fractional shortening reported in the other articles, our murine AVF model did not replicate these findings (45,187).

Specifically, while the heart rate and systolic blood pressure significantly decreased in the CJF group, our study did not reveal similar effects. Moreover, our comparative morphological analysis did not indicate significant increases in left ventricular hypertrophy based on echocardiogram examinations. Additionally, the EF reduction observed in the AVF group in the previous studies was not replicated in our model. Left ventricular perivascular staining did not show a notable increase in fibrosis in the LV vessel areas compared to the sham-operated group as reported in the other articles (45,187).

## 7. Main Findings and Conclusions

1. We could successfully establish a small-caliber AVM model in rats using the saphenous vessels.
2. During the 12-week follow-up period, shunts remained unobstructed. Systolic, diastolic, mean arterial pressure, and heart rate values slightly and non-significantly decreased in the AVM group. Echocardiogram results indicated minor systolic function impact, with slight and insignificant changes in aortic pressure and blood velocity, and minimal left ventricular wall enlargement. The small-caliber saphenous AVM model does not cause acute hemodynamic changes.
3. Moderate but progressive vascular and histological alterations, as well as venous dilatation, confirmed AVM-like features.
4. Compared to the sham-operated control group the AVM group did not show important alterations in hematological parameters nor in erythrocyte aggregation and deformability. However, slightly increased aggregation and moderately decreased deformability values were found, without significant differences. The changes normalized by the $12^{th}$ postoperative week. The alterations found were most likely related to the acute phase reactions and not to the presence of a small-caliber shunt.
5. The model seems to be suitable for studying further the progression, enlargement, or destabilization of AVM.

## 8. Summary

Developing a novel AVM model using saphenous vessels in rats constitutes a significant advancement in the study of these complex vascular anomalies. This research aimed to create a non-congenital, small-caliber AVM model, distinct from existing models that typically employ artificial arteriovenous shunts of varying sizes in different locations.

The methodology involved the meticulous construction of arteriovenous shunts on the saphenous vessels of 8 female Sprague Dawley rats, a process requiring advanced microsurgical skills and comparing the alterations to other 8 control female Sprague Dawley rats. This approach was chosen to minimize the risk of acute systemic hemodynamic changes often seen in other AVM models. Over a 12-week period, the model was closely monitored to evaluate any changes in cardiac and vascular histomorphology and micro-rheological parameters.

A key finding from this research was that the saphenous vessel AVM model did not induce the acute hemodynamic changes typically observed in other arteriovenous shunt models. However, significant alterations in certain cardiac and vascular histomorphology parameters were noted by the end of the 12-week follow-up. This included the dilatation of shunted vessels, a characteristic feature of AVMs. Interestingly, cardiomyocytes in the AVM group exhibited notable hypertrophy, characterized by an abundance of eosinophilic cytoplasm and box-like nuclei. Furthermore, the architectural layout of the myocardium appeared disordered, indicative of myocardial disarray. Despite these alterations, there was no significant evidence of myocardial fibrosis due to microvascular ischemia in any group. Additionally, the model did not result in significant micro-rheological changes. The observed changes were likely a result of acute phase reactions rather than the presence of the shunt itself. The saphenous vessel AVM model emerges as a promising tool for studying the progression, enlargement, or destabilization of AVMs under various experimental conditions, including altered angiogenesis and vascular remodeling. Its lack of acute hemodynamic and significant micro-rheological changes positions it as an ideal model for investigating AVM presence and treatment's long-term effects.

This study recommends that investigations into AVM progression, especially under varying conditions such as hypertensive or diabetic models, should begin after at least a 12-week maturation period in this model. In conclusion, this novel rat model offers a valuable pathway for enhancing our understanding of AVM pathogenesis and the effects of various interventions, while minimizing systemic circulatory impacts.

## 9. Bibliography

### 9.1. References


1. Alexander MD, Darflinger R, Cooke DL, Halbach VV. Cerebral arteriovenous fistulae. Handb Clin Neurol. 2021;176:179–98.

2. Laakso A, Hernesniemi J. Arteriovenous malformations: epidemiology and clinical presentation. Neurosurg Clin N Am. 2012 Jan;23(1):1–6.

3. Rutledge C, Cooke DL, Hetts SW, Abla AA. Brain arteriovenous malformations. Handb Clin Neurol. 2021;176:171–8.

4. Achrol AS, Guzman R, Varga M, Adler JR, Steinberg GK, Chang SD. Pathogenesis and radiobiology of brain arteriovenous malformations: implications for risk stratification in natural history and posttreatment course. Neurosurg Focus. 2009 May;26(5):E9.

5. Chen W, Choi EJ, McDougall CM, Su H. Brain arteriovenous malformation modeling, pathogenesis, and novel therapeutic targets. Transl Stroke Res. 2014 Jun;5(3):316–29.

6. Bokhari MR, Bokhari SRA. Arteriovenous Malformation Of The Brain. In: StatPearls [Internet]. Treasure Island (FL): StatPearls Publishing; 2023 [cited 2023 Mar 24]. Available from: http://www.ncbi.nlm.nih.gov/books/NBK430744/

7. Leblanc GG, Golanov E, Awad IA, Young WL, Biology of Vascular Malformations of the Brain NINDS Workshop Collaborators. Biology of vascular malformations of the brain. Stroke. 2009 Dec;40(12):e694-702.

8. Alqadi M, Brunozzi D, Linninger A, Amin-Hanjani S, Charbel FT, Alaraj A. Cerebral arteriovenous malformation venous stenosis is associated with hemodynamic changes at the draining vein-venous sinus junction. Med Hypotheses. 2019 Feb;123:86–8.

9. Halim AX, Johnston SC, Singh V, McCulloch CE, Bennett JP, Achrol AS, et al. Longitudinal risk of intracranial hemorrhage in patients with arteriovenous malformation of the brain within a defined population. Stroke. 2004 Jul;35(7):1697–702.

10. Di Rocco C, Tamburrini G, Rollo M. Cerebral Arteriovenous Malformations in Children. Acta Neurochir (Wien). 2000 Feb 1;142(2):145–58.

11. Kim H, Marchuk DA, Pawlikowska L, Chen Y, Su H, Yang G, et al. Genetic Considerations Relevant to Intracranial Hemorrhage and Brain Arteriovenous Malformations. Acta Neurochir Suppl. 2008;105:199–206.

12. Mast H, Young WL, Koennecke HC, Sciacca RR, Osipov A, Pile-Spellman J, et al. Risk of spontaneous haemorrhage after diagnosis of cerebral arteriovenous malformation. Lancet. 1997 Oct 11;350(9084):1065–8.

13. Jeffree RL, Stoodley MA. Postnatal development of arteriovenous malformations. Pediatr Neurosurg. 2009;45(4):296–304.

14. Naranbhai N, Pérez R. Management of Brain Arteriovenous Malformations: A Review. Cureus. 2023 Jan;15(1):e34053.

15. Chang W, Loecher MW, Wu Y, Niemann DB, Ciske B, Aagaard-Kienitz B, et al. Hemodynamic changes in patients with arteriovenous malformations assessed using high-resolution 3D radial phase-contrast MR angiography. AJNR Am J Neuroradiol. 2012 Sep;33(8):1565–72.

16. Ozpinar A, Mendez G, Abla AA. Epidemiology, genetics, pathophysiology, and prognostic classifications of cerebral arteriovenous malformations. Handb Clin Neurol. 2017;143:5–13.

17. Fennell VS, Martirosyan NL, Atwal GS, Kalani MYS, Ponce FA, Lemole GM, et al. Hemodynamics Associated With Intracerebral Arteriovenous Malformations: The Effects of Treatment Modalities. Neurosurgery. 2018 Oct 1;83(4):611–21.

18. Friedlander RM. Clinical practice. Arteriovenous malformations of the brain. N Engl J Med. 2007 Jun 28;356(26):2704–12.

19. Grzyska U, Fiehler J. Pathophysiology and treatment of brain AVMs. Klin Neuroradiol. 2009 Mar;19(1):82–90.

20. Hofmeister C, Stapf C, Hartmann A, Sciacca RR, Mansmann U, terBrugge K, et al. Demographic, morphological, and clinical characteristics of 1289 patients with brain arteriovenous malformation. Stroke. 2000 Jun;31(6):1307–10.

21. Rosenkranz M, Regelsberger J, Zeumer H, Grzyska U. Management of cerebral arteriovenous malformations associated with symptomatic congestive intracranial hypertension. Eur Neurol. 2008;59(1–2):62–6.

22. Qiao C, Richter GT, Pan W, Jin Y, Lin X. Extracranial arteriovenous malformations: from bedside to bench. Mutagenesis. 2019 Dec 19;34(4):299–306.

23. Timbang MR, Richter GT. Update on extracranial arteriovenous malformations: A staged multidisciplinary approach. Semin Pediatr Surg. 2020 Oct;29(5):150965.

24. Wu W, An FD, Piao CL, Tan MK, Si ZD, Xin L, et al. Management of pancreatic arteriovenous malformation: Case report and literature review. Medicine (Baltimore). 2021 Dec 23;100(51):e27983.

25. Hoang VT, Van HAT, Trinh CT, Pham NTT, Huynh C, Ha TN, et al. Uterine Arteriovenous Malformation: A Pictorial Review of Diagnosis and Management. J Endovasc Ther. 2021 Oct;28(5):659–75.

26. Lee HN, Hyun D. Pulmonary Arteriovenous Malformation and Its Vascular Mimickers. Korean J Radiol. 2022 Feb;23(2):202–17.

27. Moftakhar P, Hauptman JS, Malkasian D, Martin NA. Cerebral arteriovenous malformations. Part 2: physiology. Neurosurg Focus. 2009 May;26(5):E11.

28. Zhu Y, Lawton MT, Du R, Shwe Y, Chen Y, Shen F, et al. Expression of hypoxia-inducible factor-1 and vascular endothelial growth factor in response to venous hypertension. Neurosurgery. 2006 Sep;59(3):687–96; discussion 687-696.

29. Sure U, Battenberg E, Dempfle A, Tirakotai W, Bien S, Bertalanffy H. Hypoxia-inducible factor and vascular endothelial growth factor are expressed more frequently in embolized than in nonembolized cerebral arteriovenous malformations. Neurosurgery. 2004 Sep;55(3):663–9; discussion 669-670.

30. Ryu JY, Kim YH, Lee JS, Lee JW, Oh EJ, Kim HM, et al. Oscillatory shear stress promotes angiogenic effects in arteriovenous malformations endothelial cells. Mol Med. 2021 Mar 31;27:31.

31. Morgan MK, Johnston I, Besser M, Baines D. Cerebral arteriovenous malformations, steal, and the hypertensive breakthrough threshold. An experimental study in rats. J Neurosurg. 1987 Apr;66(4):563–7.

32. Lawton MT, Jacobowitz R, Spetzler RF. Redefined role of angiogenesis in the pathogenesis of dural arteriovenous malformations. J Neurosurg. 1997 Aug;87(2):267–74.

33. Herman JM, Spetzler RF, Bederson JB, Kurbat JM, Zabramski JM. Genesis of a dural arteriovenous malformation in a rat model. J Neurosurg. 1995 Sep;83(3):539–45.

34. Sekhon LH, Morgan MK, Spence I. Normal perfusion pressure breakthrough: the role of capillaries. J Neurosurg. 1997 Mar;86(3):519–24.

35. Yassari R, Sayama T, Jahromi BS, Aihara Y, Stoodley M, Macdonald RL. Angiographic, hemodynamic and histological characterization of an arteriovenous fistula in rats. Acta Neurochir. 2004 May 1;146(5):495–504.

36. Maruyama K, Kawahara N, Shin M, Tago M, Kishimoto J, Kurita H, et al. The risk of hemorrhage after radiosurgery for cerebral arteriovenous malformations. N Engl J Med. 2005 Jan 13;352(2):146–53.

37. Storer K, Tu J, Karunanayaka A, Smee R, Short R, Thorpe P, et al. Coadministration of low-dose lipopolysaccharide and soluble tissue factor induces thrombosis after radiosurgery in an animal arteriovenous malformation model. Neurosurgery. 2007 Sep;61(3):604–10; discussion 610-611.

38. Storer KP, Tu J, Stoodley MA, Smee RI. Expression of endothelial adhesion molecules after radiosurgery in an animal model of arteriovenous malformation. Neurosurgery. 2010 Oct;67(4):976–83; discussion 983.

39. Tu J, Karunanayaka A, Windsor A, Stoodley MA. Comparison of an animal model of arteriovenous malformation with human arteriovenous malformation. J Clin Neurosci. 2010 Jan;17(1):96–102.

40. Amal Raj J, Stoodley M. Experimental Animal Models of Arteriovenous Malformation: A Review. Vet Sci. 2015 Jun 19;2(2):97–110.

41. Bourdeau A, Dumont DJ, Letarte M. A murine model of hereditary hemorrhagic telangiectasia. J Clin Invest. 1999 Nov 15;104(10):1343–51.

42. Choi EJ, Chen W, Jun K, Arthur HM, Young WL, Su H. Novel Brain Arteriovenous Malformation Mouse Models for Type 1 Hereditary Hemorrhagic Telangiectasia. PLoS One. 2014 Feb 10;9(2):e88511.

43. Mahmoud M, Allinson KR, Zhai Z, Oakenfull R, Ghandi P, Adams RH, et al. Pathogenesis of arteriovenous malformations in the absence of endoglin. Circ Res. 2010 Apr 30;106(8):1425–33.

44. Hever T, Nemeth N, Brath E, Toth L, Kiss F, Sajtos E, et al. Morphological, hemodynamical and hemorheological changes of mature artificial saphenous arterio-venous shunts in the rat model. Microsurgery. 2010 Nov;30(8):649–56.

45. Ghanem S, Tanczos B, Deak A, Bidiga L, Nemeth N. Carotid-Jugular Fistula Model to Study Systemic Effects and Fistula-Related Microcirculatory Changes. J Vasc Res. 2018;55(5):268–77.

46. Ghanem S, Somogyi V, Tanczos B, Szabo B, Deak A, Nemeth N. Modulation of micro-rheological and hematological parameters in the presence of artificial carotid-jugular fistula in rats. Clin Hemorheol Microcirc. 2019;71(3):325–35.

47. Szabo B, Tanczos B, Varga A, Barath B, Ghanem S, Rezsabek Z, et al. Micro-Rheological Changes of Red Blood Cells in the Presence of an Arterio-Venous Fistula or a Loop-Shaped Venous Graft in the Rat. Front Physiol. 2020;11:616528.

48. Klarik Z, Toth E, Kiss F, Miko I, Furka I, Nemeth N. A modified microsurgical model for end-to-side selective portacaval shunt in the rat. Intraoperative microcirculatory investigations. Acta Cir Bras. 2013 Sep;28(9):625–31.

49. Spetzler RF, Martin NA. A proposed grading system for arteriovenous malformations. J Neurosurg. 1986 Oct;65(4):476–83.

50. Spetzler RF, Hargraves RW, McCormick PW, Zabramski JM, Flom RA, Zimmerman RS. Relationship of perfusion pressure and size to risk of hemorrhage from arteriovenous malformations. J Neurosurg. 1992 Jun;76(6):918–23.

51. Lawton MT, Kim H, McCulloch CE, Mikhak B, Young WL. A Supplementary Grading Scale for Selecting Patients with Brain Arteriovenous Malformations for Surgery. Neurosurgery. 2010 Apr;66(4):702–13.

52. Shaligram SS, Winkler E, Cooke D, Su H. Risk factors for hemorrhage of brain arteriovenous malformation. CNS Neurosci Ther. 2019 Jul 29;25(10):1085–95.

53. Spears J, Terbrugge KG, Moosavian M, Montanera W, Willinsky RA, Wallace MC, et al. A discriminative prediction model of neurological outcome for patients undergoing surgery of brain arteriovenous malformations. Stroke. 2006 Jun;37(6):1457–64.

54. Plasencia AR, Santillan A. Embolization and radiosurgery for arteriovenous malformations. Surg Neurol Int. 2012 Apr 26;3(Suppl 2):S90–104.

55. Pan P, Weinsheimer S, Cooke D, Winkler E, Abla A, Kim H, et al. Review of treatment and therapeutic targets in brain arteriovenous malformation. J Cereb Blood Flow Metab. 2021 Dec;41(12):3141–56.

56. Schimmel K, Ali MK, Tan SY, Teng J, Do HM, Steinberg GK, et al. Arteriovenous Malformations—Current Understanding of the Pathogenesis with Implications for Treatment. Int J Mol Sci. 2021 Aug 21;22(16):9037.

57. Liu AS, Mulliken JB, Zurakowski D, Fishman SJ, Greene AK. Extracranial arteriovenous malformations: natural progression and recurrence after treatment. Plast Reconstr Surg. 2010 Apr;125(4):1185–94.

58. Milic A, Chan RP, Cohen JH, Faughnan ME. Reperfusion of pulmonary arteriovenous malformations after embolotherapy. J Vasc Interv Radiol. 2005 Dec;16(12):1675–83.

59. Oulasvirta E, Niini T, Hafez A, Koroknay-Pál P, Niemelä M, Luostarinen T, et al. Correlation between arteriovenous malformation nidus size and intraparenchymal hematoma volume in the event of rupture. Brain Spine. 2022;2:101663.

60. Shakur SF, Amin-Hanjani S, Mostafa H, Charbel FT, Alaraj A. Hemodynamic Characteristics of Cerebral Arteriovenous Malformation Feeder Vessels With and Without Aneurysms. Stroke. 2015 Jul;46(7):1997–9.

61. Stefani MA, Sgarabotto Ribeiro D, Mohr JP. Grades of brain arteriovenous malformations and risk of hemorrhage and death. Ann Clin Transl Neurol. 2019 Mar;6(3):508–14.

62. Boster KAS, Shidhore TC, Cohen-Gadol AA, Christov IC, Rayz VL. Challenges in Modeling Hemodynamics in Cerebral Aneurysms Related to Arteriovenous Malformations. Cardiovasc Eng Technol. 2022 Oct;13(5):673–84.

63. Lawton MT, Rutledge WC, Kim H, Stapf C, Whitehead KJ, Li DY, et al. Brain arteriovenous malformations. Nat Rev Dis Primers. 2015 May 28;1(1):1–20.

64. Kim H, Su H, Weinsheimer S, Pawlikowska L, Young WL. Brain arteriovenous malformation pathogenesis: a response-to-injury paradigm. Acta Neurochir Suppl. 2011;111:83–92.

65. Valavanis A, Pangalu A, Tanaka M. Endovascular treatment of cerebral arteriovenous malformations with emphasis on the curative role of embolisation. Interv Neuroradiol. 2005 Oct 5;11(Suppl 1):37–43.

66. Geibprasert S, Pongpech S, Jiarakongmun P, Shroff MM, Armstrong DC, Krings T. Radiologic assessment of brain arteriovenous malformations: what clinicians need to know. Radiographics. 2010 Mar;30(2):483–501.

67. Kim EJ, Vermeulen S, Li FJ, Newell DW. A review of cerebral arteriovenous malformations and treatment with stereotactic radiosurgery. Translational Cancer Research [Internet]. 2014 Aug [cited 2024 Jan 14];3(4). Available from: https://tcr.amegroups.org/article/view/2951

68. Berman MF, Sciacca RR, Pile-Spellman J, Stapf C, Connolly ES, Mohr JP, et al. The epidemiology of brain arteriovenous malformations. Neurosurgery. 2000 Aug;47(2):389–96; discussion 397.

69. Fullerton HJ, Achrol AS, Johnston SC, McCulloch CE, Higashida RT, Lawton MT, et al. Long-term hemorrhage risk in children versus adults with brain arteriovenous malformations. Stroke. 2005 Oct;36(10):2099–104.

70. Brown RD, Wiebers DO, Torner JC, O'Fallon WM. Frequency of intracranial hemorrhage as a presenting symptom and subtype analysis: a population-based study of intracranial vascular malformations in Olmsted Country, Minnesota. J Neurosurg. 1996 Jul;85(1):29–32.

71. Al-Shahi R, Fang JSY, Lewis SC, Warlow CP. Prevalence of adults with brain arteriovenous malformations: a community based study in Scotland using capture-recapture analysis. J Neurol Neurosurg Psychiatry. 2002 Nov;73(5):547–51.

72. Jessurun GA, Kamphuis DJ, van der Zande FH, Nossent JC. Cerebral arteriovenous malformations in The Netherlands Antilles. High prevalence of hereditary hemorrhagic telangiectasia-related single and multiple cerebral arteriovenous malformations. Clin Neurol Neurosurg. 1993 Sep;95(3):193–8.

73. Kim T, Kwon OK, Bang JS, Lee H, Kim JE, Kang HS, et al. Epidemiology of ruptured brain arteriovenous malformation: a National Cohort Study in Korea. J Neurosurg. 2018 Jun 1;1–6.

74. Morris Z, Whiteley WN, Longstreth WT, Weber F, Lee YC, Tsushima Y, et al. Incidental findings on brain magnetic resonance imaging: systematic review and meta-analysis. BMJ. 2009 Aug 17;339:b3016.

75. Ajiboye N, Chalouhi N, Starke RM, Zanaty M, Bell R. Cerebral arteriovenous malformations: evaluation and management. ScientificWorldJournal. 2014;2014:649036.

76. Robinson JR, Awad IA, Little JR. Natural history of the cavernous angioma. J Neurosurg. 1991 Nov;75(5):709–14.

77. van Beijnum J, van der Worp HB, Buis DR, Al-Shahi Salman R, Kappelle LJ, Rinkel GJE, et al. Treatment of brain arteriovenous malformations: a systematic review and meta-analysis. JAMA. 2011 Nov 9;306(18):2011–9.

78. Jordan LC, Hillis AE. Hemorrhagic stroke in children. Pediatr Neurol. 2007 Feb;36(2):73–80.

79. Tatlisumak T, Cucchiara B, Kuroda S, Kasner SE, Putaala J. Nontraumatic intracerebral haemorrhage in young adults. Nat Rev Neurol. 2018 Apr;14(4):237–50.

80. Gross BA, Du R. Natural history of cerebral arteriovenous malformations: a meta-analysis. J Neurosurg. 2013 Feb;118(2):437–43.

81. Brown RD, Wiebers DO, Forbes G, O'Fallon WM, Piepgras DG, Marsh WR, et al. The natural history of unruptured intracranial arteriovenous malformations. J Neurosurg. 1988 Mar;68(3):352–7.

82. Ondra SL, Troupp H, George ED, Schwab K. The natural history of symptomatic arteriovenous malformations of the brain: a 24-year follow-up assessment. J Neurosurg. 1990 Sep;73(3):387–91.

83. Herzig R, Bogousslavsky J, Maeder P, Maeder-Ingvar M, Reichhart M, Urbano LA, et al. Intracranial arterial and arteriovenous malformations presenting with infarction. Lausanne Stroke Registry study. Eur J Neurol. 2005 Feb;12(2):93–102.

84. Rutledge WC, Ko NU, Lawton MT, Kim H. Hemorrhage rates and risk factors in the natural history course of brain arteriovenous malformations. Transl Stroke Res. 2014 Oct;5(5):538–42.

85. Liu YT, Yang TC, Jung SM, Lee CC. Probable pathogenesis, diagnosis, and management of untreated arteriovenous malformation with cyst formation: case report and literature review. Acta Neurol Belg. 2018 Dec;118(4):603–5.

86. Shaligram SS, Winkler E, Cooke D, Su H. Risk factors for hemorrhage of brain arteriovenous malformation. CNS Neurosci Ther. 2019 Oct;25(10):1085–95.

87. Ferrara AR. Brain arteriovenous malformations. Radiol Technol. 2011;82(6):543MR-56MR.

88. Gailloud P. Endovascular treatment of cerebral arteriovenous malformations. Tech Vasc Interv Radiol. 2005 Sep;8(3):118–28.

89. Novakovic RL, Lazzaro MA, Castonguay AC, Zaidat OO. The diagnosis and management of brain arteriovenous malformations. Neurol Clin. 2013 Aug;31(3):749–63.

90. Mullan S, Mojtahedi S, Johnson DL, Macdonald RL. Embryological basis of some aspects of cerebral vascular fistulas and malformations. J Neurosurg. 1996 Jul;85(1):1–8.

91. Tasiou A, Tzerefos C, Alleyne CH, Boccardi E, Karlsson B, Kitchen N, et al. Arteriovenous Malformations: Congenital or Acquired Lesions? World Neurosurg. 2020 Feb;134:e799–807.

92. Barbosa Do Prado L, Han C, Oh SP, Su H. Recent Advances in Basic Research for Brain Arteriovenous Malformation. Int J Mol Sci. 2019 Oct 25;20(21):5324.

93. Winkler EA, Pacult MA, Catapano JS, Scherschinski L, Srinivasan VM, Graffeo CS, et al. Emerging pathogenic mechanisms in human brain arteriovenous malformations: a contemporary review in the multiomics era. Neurosurg Focus. 2022 Jul;53(1):E2.

94. Hashimoto T, Mesa-Tejada R, Quick CM, Bollen AW, Joshi S, Pile-Spellman J, et al. Evidence of increased endothelial cell turnover in brain arteriovenous malformations. Neurosurgery. 2001 Jul;49(1):124–31; discussion 131-132.

95. Uranishi R, Baev NI, Kim JH, Awad IA. Vascular smooth muscle cell differentiation in human cerebral vascular malformations. Neurosurgery. 2001 Sep;49(3):671–9; discussion 679-680.

96. Pawlikowska L, Tran MN, Achrol AS, Ha C, Burchard E, Choudhry S, et al. Polymorphisms in transforming growth factor-beta-related genes ALK1 and ENG are associated with sporadic brain arteriovenous malformations. Stroke. 2005 Oct;36(10):2278–80.

97. Dalton A, Dobson G, Prasad M, Mukerji N. De novo intracerebral arteriovenous malformations and a review of the theories of their formation. Br J Neurosurg. 2018 Jun;32(3):305–11.

98. Nikolaev SI, Vetiska S, Bonilla X, Boudreau E, Jauhiainen S, Rezai Jahromi B, et al. Somatic Activating KRAS Mutations in Arteriovenous Malformations of the Brain. N Engl J Med. 2018 Jan 18;378(3):250–61.

99. Couto JA, Huang AY, Konczyk DJ, Goss JA, Fishman SJ, Mulliken JB, et al. Somatic MAP2K1 Mutations Are Associated with Extracranial Arteriovenous Malformation. Am J Hum Genet. 2017 Mar 2;100(3):546–54.

100. Tu J, Stoodley MA, Morgan MK, Storer KP. Ultrastructure of perinidal capillaries in cerebral arteriovenous malformations. Neurosurgery. 2006 May;58(5):961–70; discussion 961-970.

101. Chen W, Guo Y, Walker EJ, Shen F, Jun K, Oh SP, et al. Reduced mural cell coverage and impaired vessel integrity after angiogenic stimulation in the Alk1-deficient brain. Arterioscler Thromb Vasc Biol. 2013 Feb;33(2):305–10.

102. Sure U, Butz N, Schlegel J, Siegel AM, Wakat JP, Mennel HD, et al. Endothelial proliferation, neoangiogenesis, and potential de novo generation of cerebrovascular malformations. J Neurosurg. 2001 Jun;94(6):972–7.

103. Sweeney MD, Zhao Z, Montagne A, Nelson AR, Zlokovic BV. Blood-Brain Barrier: From Physiology to Disease and Back. Physiol Rev. 2019 Jan 1;99(1):21–78.

104. Winkler EA, Lu AY, Raygor KP, Linzey JR, Jonzzon S, Lien BV, et al. Defective vascular signaling & prospective therapeutic targets in brain arteriovenous malformations. Neurochem Int. 2019 Jun;126:126–38.

105. Winkler EA, Birk H, Burkhardt JK, Chen X, Yue JK, Guo D, et al. Reductions in brain pericytes are associated with arteriovenous malformation vascular instability. J Neurosurg. 2018 Dec 1;129(6):1464–74.

106. Moftakhar P, Hauptman JS, Malkasian D, Martin NA. Cerebral arteriovenous malformations. Part 1: cellular and molecular biology. Neurosurg Focus. 2009 May;26(5):E10.

107. Yaşargil MG. A legacy of microneurosurgery: memoirs, lessons, and axioms. Neurosurgery. 1999 Nov;45(5):1025–92.

108. Thomas JM, Surendran S, Abraham M, Sasankan D, Bhaadri S, Rajavelu A, et al. Gene expression analysis of nidus of cerebral arteriovenous malformations reveals vascular structures with deficient differentiation and maturation. PLoS One. 2018;13(6):e0198617.

109. Hashimoto N, Nozaki K. Do cerebral arteriovenous malformations recur after angiographically confirmed total extirpation? Crit Rev Neurosurg. 1999 May 25;9(3):141–6.

110. Mohr JP, Overbey JR, Hartmann A, Kummer R von, Al-Shahi Salman R, Kim H, et al. Medical management with interventional therapy versus medical management alone for unruptured brain arteriovenous malformations (ARUBA): final follow-up of a multicentre, non-blinded, randomised controlled trial. Lancet Neurol. 2020 Jul;19(7):573–81.

111. Mohr JP, Parides MK, Stapf C, Moquete E, Moy CS, Overbey JR, et al. Medical management with or without interventional therapy for unruptured brain arteriovenous malformations (ARUBA): a multicentre, non-blinded, randomised trial. Lancet. 2014 Feb 15;383(9917):614–21.

112. Dicpinigaitis AJ, Ogulnick JV, Mayer SA, Gandhi CD, Al-Mufti F. Increase in Ruptured Cerebral Arteriovenous Malformations and Mortality in the United States: Unintended Consequences of the ARUBA Trial? Stroke: Vascular and Interventional Neurology. 2023 Jan;3(1):e000442.

113. Wu EM, El Ahmadieh TY, McDougall CM, Aoun SG, Mehta N, Neeley OJ, et al. Embolization of brain arteriovenous malformations with intent to cure: a systematic review. J Neurosurg. 2019 Feb 1;132(2):388–99.

114. Heit JJ, Thakur NH, Iv M, Fischbein NJ, Wintermark M, Dodd RL, et al. Arterial-spin labeling MRI identifies residual cerebral arteriovenous malformation following stereotactic radiosurgery treatment. J Neuroradiol. 2020 Feb;47(1):13–9.

115. Ironside N, Chen CJ, Ding D, Ilyas A, Kumar JS, Buell TJ, et al. Seizure Outcomes After Radiosurgery for Cerebral Arteriovenous Malformations: An Updated Systematic Review and Meta-Analysis. World Neurosurg. 2018 Dec;120:550-562.e3.

116. Kocer N, Kandemirli SG, Dashti R, Kizilkilic O, Hanimoglu H, Sanus GZ, et al. Single-stage planning for total cure of grade III-V brain arteriovenous malformations by embolization alone or in combination with microsurgical resection. Neuroradiology. 2019 Feb;61(2):195–205.

117. Quintin S, Figg JW, Mehkri Y, Hanna CO, Woolridge MG, Lucke-Wold B. Arteriovenous Malformations: An Update on Models and Therapeutic Targets. J Neurosci Neurol Surg. 2023;13(1):250.

118. Beck CS, McKHANN CF, Belnap WD. Revascularization of the brain through establishment of a cervical arteriovenous fistula; effects in children with mental retardation and convulsive disorders. J Pediatr. 1949 Sep;35(3):317–29.

119. Scott BB, McGillicuddy JE, Seeger JF, Kindt GW, Giannotta SL. Vascular dynamics of an experimental cerebral arteriovenous shunt in the primate. Surg Neurol. 1978 Jul;10(1):34–8.

120. Wang N, Chen YN, Zhang L, Li Y, Liu SS, Zhan HF, et al. Isothermal Diffusion Behavior and Surface Performance of Cu/Ni Coating on TC4 Alloy. Materials (Basel). 2019 Nov 24;12(23):3884.

121. Morgan MK, Anderson RE, Sundt TM. A model of the pathophysiology of cerebral arteriovenous malformations by a carotid-jugular fistula in the rat. Brain Research. 1989 Sep 4;496(1):241–50.

122. Qian Z, Climent S, Maynar M, Usón-Garallo J, Lima-Rodrigues MA, Calles C, et al. A simplified arteriovenous malformation model in sheep: feasibility study. AJNR Am J Neuroradiol. 1999 May;20(5):765–70.

123. Altschuler E, Lunsford LD, Kondziolka D, Wu A, Maitz AH, Sclabassi R, et al. Radiobiologic models for radiosurgery. Neurosurg Clin N Am. 1992 Jan;3(1):61–77.

124. Pietilä TA, Zabramski JM, Thèllier-Janko A, Duveneck K, Bichard WD, Brock M, et al. Animal model for cerebral arteriovenous malformation. Acta Neurochir (Wien). 2000;142(11):1231–40.

125. Chaloupka JC, Viñuela F, Robert J, Duckwiler GR. An in vivo arteriovenous malformation model in swine: preliminary feasibility and natural history study. AJNR Am J Neuroradiol. 1994 May;15(5):945–50.

126. Wakhloo AK, Lieber BB, Siekmann R, Eber DJ, Gounis MJ. Acute and chronic swine rete arteriovenous malformation models: hemodynamics and vascular remodeling. AJNR Am J Neuroradiol. 2005 Aug;26(7):1702–6.

127. Massoud TF, Ji C, Viñuela F, Guglielmi G, Robert J, Duckwiler GR, et al. An experimental arteriovenous malformation model in swine: anatomic basis and construction technique. American Journal of Neuroradiology. 1994 Sep 1;15(8):1537–45.

128. Lieber BB, Wakhloo AK, Siekmann R, Gounis MJ. Acute and chronic swine rete arteriovenous malformation models: effect of ethiodol and glacial acetic acid on penetration, dispersion, and injection force of N-butyl 2-cyanoacrylate. AJNR Am J Neuroradiol. 2005 Aug;26(7):1707–14.

129. Lylyk P, Viñuela F, Vinters HV, Dion J, Bentson J, Duckwiler G, et al. Use of a new mixture for embolization of intracranial vascular malformations. Preliminary experimental experience. Neuroradiology. 1990;32(4):304–10.

130. Li W, Liang S, Zhang W, Zhao X, Zhang H, Lv X. Liquid embolic agent Fe3O4-EVOH for endovascular arteriovenous malformation embolisation: Preliminary evaluation in an in vivo swine rete mirabile model. Neuroradiol J. 2020 Aug;33(4):306–10.

131. Satomi J, Mount RJ, Toporsian M, Paterson AD, Wallace MC, Harrison RV, et al. Cerebral vascular abnormalities in a murine model of hereditary hemorrhagic telangiectasia. Stroke. 2003 Mar;34(3):783–9.

132. Choi EJ, Chen W, Jun K, Arthur HM, Young WL, Su H. Novel Brain Arteriovenous Malformation Mouse Models for Type 1 Hereditary Hemorrhagic Telangiectasia. PLOS ONE. 2014 Feb 10;9(2):e88511.

133. Xu B, Wu YQ, Huey M, Arthur HM, Marchuk DA, Hashimoto T, et al. Vascular endothelial growth factor induces abnormal microvasculature in the endoglin heterozygous mouse brain. J Cereb Blood Flow Metab. 2004 Feb;24(2):237–44.

134. Johnson DW, Berg JN, Baldwin MA, Gallione CJ, Marondel I, Yoon SJ, et al. Mutations in the activin receptor-like kinase 1 gene in hereditary haemorrhagic telangiectasia type 2. Nat Genet. 1996 Jun;13(2):189–95.

135. Han C, Lang MJ, Nguyen CL, Luna Melendez E, Mehta S, Turner GH, et al. Novel experimental model of brain arteriovenous malformations using conditional Alk1 gene deletion in transgenic mice. J Neurosurg. 2021 Nov 5;1–12.

136. Walker EJ, Su H, Shen F, Choi EJ, Oh SP, Chen G, et al. Arteriovenous malformation in the adult mouse brain resembling the human disease. Ann Neurol. 2011 Jun;69(6):954–62.

137. Milton I, Ouyang D, Allen CJ, Yanasak NE, Gossage JR, Alleyne CH, et al. Age-dependent lethality in novel transgenic mouse models of central nervous system arteriovenous malformations. Stroke. 2012 May;43(5):1432–5.

138. Carvalho RLC, Itoh F, Goumans MJ, Lebrin F, Kato M, Takahashi S, et al. Compensatory signalling induced in the yolk sac vasculature by deletion of TGFbeta receptors in mice. J Cell Sci. 2007 Dec 15;120(Pt 24):4269–77.

139. Su H, Kim H, Pawlikowska L, Kitamura H, Shen F, Cambier S, et al. Reduced expression of integrin alphavbeta8 is associated with brain arteriovenous malformation pathogenesis. Am J Pathol. 2010 Feb;176(2):1018–27.

140. Fish JE, Flores Suarez CP, Boudreau E, Herman AM, Gutierrez MC, Gustafson D, et al. Somatic Gain of KRAS Function in the Endothelium Is Sufficient to Cause Vascular Malformations That Require MEK but Not PI3K Signaling. Circ Res. 2020 Aug 28;127(6):727–43.

141. Park ES, Kim S, Huang S, Yoo JY, Körbelin J, Lee TJ, et al. Selective Endothelial Hyperactivation of Oncogenic KRAS Induces Brain Arteriovenous Malformations in Mice. Ann Neurol. 2021 May;89(5):926–41.

142. Murphy PA, Lam MTY, Wu X, Kim TN, Vartanian SM, Bollen AW, et al. Endothelial Notch4 signaling induces hallmarks of brain arteriovenous malformations in mice. Proc Natl Acad Sci U S A. 2008 Aug 5;105(31):10901–6.

143. Nielsen CM, Cuervo H, Ding VW, Kong Y, Huang EJ, Wang RA. Deletion of Rbpj from postnatal endothelium leads to abnormal arteriovenous shunting in mice. Development. 2014 Oct;141(19):3782–92.

144. Amili O, Schiavazzi D, Moen S, Jagadeesan B, Van de Moortele PF, Coletti F. Hemodynamics in a giant intracranial aneurysm characterized by in vitro 4D flow MRI. PLoS One. 2018;13(1):e0188323.

145. Ishikawa M, Horikawa M, Yamagami T, Uchida BT, Awai K, Kaufman JA. Embolization of Arteriovenous Malformations: Effect of Flow Control and Composition of n-Butyl-2 Cyanoacrylate and Iodized Oil Mixtures with and without Ethanol in an in Vitro Model. Radiology. 2016 Jun;279(3):910–6.

146. Inagawa S, Isoda H, Kougo H, Isogais S, Sakahara H. In-Vitro Simulation of NBCA Embolization for Arteriovenous Malformation. Interv Neuroradiol. 2003 Dec 20;9(4):351–8.

147. Kaneko N, Ullman H, Ali F, Berg P, Ooi YC, Tateshima S, et al. In Vitro Modeling of Human Brain Arteriovenous Malformation for Endovascular Simulation and Flow Analysis. World Neurosurg. 2020 Sep;141:e873–9.

148. Soon K, Li M, Wu R, Zhou A, Khosraviani N, Turner WD, et al. A human model of arteriovenous malformation (AVM)-on-a-chip reproduces key disease hallmarks and enables drug testing in perfused human vessel networks. Biomaterials. 2022 Sep;288:121729.

149. Pollock BE, Flickinger JC. A proposed radiosurgery-based grading system for arteriovenous malformations. J Neurosurg. 2002 Jan;96(1):79–85.

150. Starke RM, Komotar RJ, Otten ML, Hahn DK, Fischer LE, Hwang BY, et al. Adjuvant embolization with N-butyl cyanoacrylate in the treatment of cerebral arteriovenous malformations: outcomes, complications, and predictors of neurologic deficits. Stroke. 2009 Aug;40(8):2783–90.

151. Finkelstein A. Design and evaluation of a new diagnostic instrument for osmotic gradient ektacytometrie. Electronics, Université Paris-Es. 2017;

152. Hardeman MR, Goedhart PeterT, Shin S. Methods in hemorheology. In: Baskurt OK, Hardeman MR, Rampling MW, Meiselman HJ, editors. Handbook of hemorheology and hemodynamics. Amsterdam: IOS Press; 2007. p. 242–66.

153. Baskurt OK, Hardeman MR, Uyuklu M, Ulker P, Cengiz M, Nemeth N, et al. Parameterization of red blood cell elongation index – shear stress curves obtained by ektacytometry. Scandinavian Journal of Clinical and Laboratory Investigation. 2009;69(7):777–88.

154. Baskurt OK, Meiselman HJ. Data reduction methods for ektacytometry in clinical hemorheology. Clinical hemorheology and microcirculation. 2013 Jan 1;54(1):99–107.

155. Yamamoto K, Li X, Shu C, Miyata T, Dardik A. Technical aspects of the mouse aortocaval fistula. Journal of visualized experiments : JoVE. 2013;(77):50449.

156. Zheng C, Zhou Y, Huang C, Zhang Z, Liu YI, Xu Y. Establishment of a rat autogenous arteriovenous fistula model following 5/6 nephrectomy. Experimental and therapeutic medicine. 2015 Jul;10(1):219–24.

157. Sageshima M, Kawamura K, Toda K, Masuda H, Shozawa T. An ultrastructural study of pulmonary capillary vessels in blood volume-overloaded rat. Advances in experimental medicine and biology. 1990;277:673–80.

158. Tohda K, Masuda H, Kawamura K, Shozawa T. Difference in dilatation between endothelium-preserved and -desquamated segments in the flow-loaded rat common carotid artery. Arteriosclerosis and thrombosis : a journal of vascular biology. 1992 Apr;12(4):519–28.

159. Geenen IL, Kolk FF, Molin DG, Wagenaar A, Compeer MG, Tordoir JH, et al. Nitric Oxide Resistance Reduces Arteriovenous Fistula Maturation in Chronic Kidney Disease in Rats. Jourd'heuil D, editor. PloS one. 2016 Jan 4;11(1):e0146212.

160. Chou TF, Chen YS, Yu CC, Chien CT, Chen CF. Simple methods to elevate pulmonary arterial pressure by pre- and post-tricuspid shunts in rats. The Chinese journal of physiology. 2002 Sep 30;45(3):131–5.

161. Wang X, Ren B, Liu S, Sentex E, Tappia PS, Dhalla NS. Characterization of cardiac hypertrophy and heart failure due to volume overload in the rat. Journal of Applied Physiology. 2003;94(2):752–63.

162. Liu Z, Hilbelink DR, Crockett WB, Gerdes AM. Regional changes in hemodynamics and cardiac myocyte size in rats with aortocaval fistulas. 1. Developing and established hypertrophy. Circulation research. 1991 Jul;69(1):52–8.

163. Ozek C, Zhang F, Lineaweaver WC, Chin BT, Eiman T, Newlin L, et al. A new heart failure model in rat by an end-to-side femoral vessel anastomosis. Cardiovascular research. 1998 Jan;37(1):236–8.

164. Langer S, Heiss C, Paulus N, Bektas N, Mommertz G, Rowinska Z, et al. Functional and structural response of arterialized femoral veins in a rodent AV fistula model. Nephrology Dialysis Transplantation. 2009 Jul;24(7):2201–6.

165. Hever T, Nemeth N, Brath E, Toth L, Kiss F, Sajtos E, et al. Morphological, hemodynamical and hemorheological changes of mature artificial saphenous arterio-venous shunts in the rat model. Microsurgery. 2010 Nov;30(8):649–56.

166. Lv M ming, Fan X dong, Su L xin. Is a swine model of arteriovenous malformation suitable for human extracranial arteriovenous malformation? A preliminary study. Cardiovasc Intervent Radiol. 2013 Oct;36(5):1364–70.

167. Klisch J, Requejo F, Yin L, Eissner B, Schumacher M. The two-in-one model: a new variation of the arteriovenous malformation model in swine. Neuroradiology. 2001 May;43(5):393–7.

168. Xu M, Xu H, Qin Z. Animal Models in Studying Cerebral Arteriovenous Malformation. Biomed Res Int. 2015;2015:178407.

169. Spetzler RF, Wilson CB, Weinstein P, Mehdorn M, Townsend J, Telles D. Normal perfusion pressure breakthrough theory. Clin Neurosurg. 1978;25:651–72.

170. Sakaki T, Tsujimoto S, Nishitani M, Ishida Y, Morimoto T. Perfusion pressure breakthrough threshold of cerebral autoregulation in the chronically ischemic brain: an experimental study in cats. J Neurosurg. 1992 Mar;76(3):478–85.

171. Tokiwa K, Miyasaka Y, Irikura K, Tanaka R, Yamada M. The effects of a carotid-jugular fistula on cerebral blood flow in the cat: an experimental study in the chronic period. Neurol Res. 1995 Aug;17(4):297–300.

172. Morgan MK, Anderson RE, Sundt TM. The effects of hyperventilation on cerebral blood flow in the rat with an open and closed carotid-jugular fistula. Neurosurgery. 1989 Oct;25(4):606–11; discussion 611-612.

173. Morgan WR, Majeski JA. Idiopathic arteriovenous renal vascular malformation treated by ex vivo repair. J S C Med Assoc. 1989 Oct;85(10):469–71.

174. Numazawa S, Sasaki T, Sato S, Watanabe Y, Watanabe Z, Kodama N. Experimental Model of Intracranial Arteriovenous Shunting in the Acute Stage. Neurologia medico-chirurgica. 2005;45(6):288–93.

175. Spetzler RF, Hargraves RW, McCormick PW, Zabramski JM, Flom RA, Zimmerman RS. Relationship of perfusion pressure and size to risk of hemorrhage from arteriovenous malformations. J Neurosurg. 1992 Jun;76(6):918–23.

176. Simons M, Morgan MK, Davidson AS. Cohort studies, trials, and tribulations: systematic review and an evidence-based approach to arteriovenous malformation treatment. J Neurosurg Sci. 2018 Aug;62(4):444–53.

177. Koppensteiner R. Blood rheology in emergency medicine. Semin Thromb Hemost. 1996;22(1):89–91.

178. Baskurt OK. Mechanisms of blood rheology alterations. In: Baskurt OK, Hardeman MR, Rampling MW, Meiselman HJ, editors. Handbook of hemorheology and hemodynamics. Amsterdam: IOS Press; 2007. p. 170–90.

179. Nemeth N, Deak A, Szentkereszty Z, Peto K. Effects and influencing factors on hemorheological variables taken into consideration in surgical pathophysiology research. Clin Hemorheol Microcirc. 2018;69(1–2):133–40.

180. Baskurt OK, Meiselman HJ. Red blood cell mechanical stability test. Clin Hemorheol Microcirc. 2013;55(1):55–62.

181. Szabo B, Gasz B, Fazekas LA, Varga A, Kiss-Papai L, Matolay O, et al. Heterogeneous Maturation of Arterio-Venous Fistulas and Loop-Shaped Venous Interposition Grafts: A Histological and 3D Flow Simulation Comparison. Biomedicines. 2022 Jun 25;10(7):1508.

182. Mahendra Y, He M, Rouf MA, Tjakra M, Fan L, Wang Y, et al. Progress and prospects of mechanotransducers in shear stress-sensitive signaling pathways in association with arteriovenous malformation. Clin Biomech (Bristol, Avon). 2021 Aug;88:105417.

183. Langenickel T, Pagel I, Höhnel K, Dietz R, Willenbrock R. Differential regulation of cardiac ANP and BNP mRNA in different stages of experimental heart failure. American journal of physiology Heart and circulatory physiology. 2000 May;278(5):1500–6.

184. Huang M, LeBlanc MH, Hester RL. Evaluation of the needle technique for producing an arteriovenous fistula. Journal of applied physiology (Bethesda, Md : 1985). 1994 Dec;77(6):2907–11.

185. Brower GL, Janicki JS. Contribution of ventricular remodeling to pathogenesis of heart failure in rats. American Journal of Physiology - Heart and Circulatory Physiology. 2001;280(2):674–83.

186. Treskatsch S, Feldheiser A, Rosin AT, Sifringer M, Habazettl H, Mousa SA, et al. A modified approach to induce predictable congestive heart failure by volume overload in rats. PLoS ONE. 2014;9(1):1–7.

187. Ingle K, Pham L, Lee V, Guo L, Isayeva-Waldrop T, Somarathna M, et al. Cardiac Changes Following Arteriovenous Fistula Creation in a Mouse Model. J Vasc Access. 2023 Jan;24(1):124–32.

## 9.2. Certified publication list

UNIVERSITY of DEBRECEN

UNIVERSITY AND NATIONAL LIBRARY
UNIVERSITY OF DEBRECEN
H-4002 Egyetem tér 1, Debrecen
Phone: +3652/410-443, email: publikaciok@lib.unideb.hu

Registry number: DEENK/24/2024.PL
Subject: PhD Publication List

Candidate: Mohammad Walid Al-Smadi
Doctoral School: Kálmán Laki Doctoral School

### List of publications related to the dissertation

1. **Al-Smadi, M. W.**, Fazekas, L., Varga, Á., Mátrai, Á. A., Aslan, S., Beqain, A., Al-Khafaji, M. Q. M., Baráth, B., Novák, L., Németh, N.: Minor micro-rheological alterations in the presence of an artificial saphenous arteriovenous shunt, as an arteriovenous malformation model in the rat. *Clin. Hemorheol. Microcirc. [Epub ahead of print]*, 2024.
   DOI: http://dx.doi.org/10.3233/CH-231825
   IF: 2.1 (2022)
2. **Al-Smadi, M. W.**, Fazekas, L., Aslan, S., Bernát, B., Beqain, A., Al-Khafaji, M. Q. M., Priksz, D., Orlik, B., Németh, N.: A Microsurgical Arteriovenous Malformation Model on Saphenous Vessels in the Rat.
   *Biomedicines. 11*, 1-14, 2023.
   DOI: http://dx.doi.org/10.3390/biomedicines11112970
   IF: 4.7 (2022)

### List of other publications

3. Aslan, S., **Al-Smadi, M. W.**, Kozma, I., Viola, Á.: Enhanced Precision and Safety in Thermal Ablation: O-Arm Cone Beam Computed Tomography with Magnetic Resonance Imaging Fusion for Spinal Column Tumor Targeting.
   *Cancers (Basel). 15* (24), 1-12, 2023.
   DOI: http://dx.doi.org/10.3390/cancers15245744
   IF: 5.2 (2022)
4. **Al-Smadi, M. W.**, Kozma, I., Aslan, S., Bölöni, B., Viola, Á.: Percutaneous Superimposed O-Arm-MRI-Navigated Biopsy for Spinal Column Pathologies.
   *Diagnostics. 13* (13), 1-9, 2023.
   DOI: http://dx.doi.org/10.3390/diagnostics13132252
   IF: 3.6 (2022)

DEBRECENI EGYETEM Egyetemi és Nemzeti Könyvtár

UNIVERSITY AND NATIONAL LIBRARY
UNIVERSITY OF DEBRECEN
H-4002 Egyetem tér 1, Debrecen
Phone: +3652/410-443, email: publikaciok@lib.unideb.hu

5. Szabó, B., Gasz, B., Fazekas, L., Varga, Á., Kiss-Pápai, L., Matolay, O., Rezsabek, Z., **Al-Smadi, M. W.**, Németh, N.: Heterogeneous Maturation of Arterio-Venous Fistulas and Loop-Shaped Venous Interposition Grafts: a Histological and 3D Flow Simulation Comparison.
*Biomedicines. 10*, 1-14, 2022.
DOI: http://dx.doi.org/10.3390/biomedicines10071508
IF: 4.7

6. Szabó, B., Tánczos, B., Varga, Á., Baráth, B., Ghanem, S., Rezsabek, Z., **Al-Smadi, M. W.**, Németh, N.: Micro-rheological changes of red blood cells in the presence of an arterio-venous fistula or a loop-shaped venous graft in the rat.
*Front. Physiol. 11*, 1-12, 2020.
DOI: http://dx.doi.org/10.3389/fphys.2020.616528
IF: 4.566

**Total IF of journals (all publications): 24,866**
**Total IF of journals (publications related to the dissertation): 6,8**

The Candidate's publication data submitted to the iDEa Tudóstér have been validated by DEENK on the basis of the Journal Citation Report (Impact Factor) database.

26 January, 2024

DEBRECENI EGYETEM * Egyetemi és Nemzeti Könyvtár *

## 10. Keywords

arteriovenous malformation
arteriovenous shunt
experimental model
hemodynamics
hemorheology
microsurgery
microsurgical model
vascular remodeling

## 11. Acknowledgements

I would like to express my deepest appreciation to Prof. Dr. Norbert Nemeth, whose unwavering guidance and mentorship have been the bedrock of my academic and professional journey. His insightful advice, thoughtful critique, and constant encouragement have been a source of inspiration and motivation throughout my PhD studies. Prof. Nemeth's mentorship, which started during my initial years as a medical student, has significantly shaped my approach to research and clinical practice.

A special and heartfelt thanks to my wife, Dr. Siran Aslan, for her endless support, encouragement, and sacrifice. Her understanding, patience, and belief in my abilities have been crucial in overcoming the challenges of completing my PhD studies. Her love and companionship have been a constant source of comfort and strength. Her sacrifices, particularly in balancing her own professional commitments while providing me with unwavering support, have been invaluable.

My sincere gratitude extends to the Department of Operative Techniques and Surgical Research, especially to Dr. Laszlo Fazekas. His friendship, professional collaboration, and intellectual partnership have greatly contributed to the success of my research. Working alongside Dr. Fazekas has not only enriched my professional experience but has also provided a supportive and collaborative environment that is fundamental to academic success.

I am deeply thankful to my parents, Dr. Walid and Monira Al-Smadi, for instilling in me the values of hard work and perseverance. Their lifelong dedication to my upbringing and education has been the foundation of my achievements. Their love and wisdom have always guided me. Additionally, my siblings Dina, Yazan, and Donia deserve special mention for their constant support, encouragement, and belief in my dreams. Their presence in my life has been a source of joy and inspiration.

The journey through my PhD has been a transformative experience, made possible by the unwavering support of these remarkable individuals. I am profoundly grateful for their contributions to my life and career.

## 12. Appendix

**Copies of the articles that serve as basis of this PhD dissertation**